Combining topology and fractal dimension of fracture networks characterises structural domains in thrusted limestones

Mark W. Grodner * [a], Stuart M. Clarke [a], Stuart D. Burley [a, b], A. Graham Leslie [a, c], Richard Haslam [a, d]

[a] Basin Dynamics Research Group, School of Geography, Geology and the Environment, Keele University, Keele, ST5 5BG, United Kingdom, m.w.grodner@keele.ac.uk, +44 (0) 1782 734301
s.m.clarke@keele.ac.uk

[b] Discovery Geoscience, Lapworth Croft Lodge, Lapworth, United Kingdom, stuart.burley@discovery-geoscience.com

[c] British Geological Survey, Lyell Centre, Research Avenue South, Edinburgh EH14 4AP, United Kingdom, agle@bgs.ac.uk

[d] British Geological Survey, Keyworth Centre, Nicker Hill, Keyworth, Nottingham NG12 5GG, United Kingdom, richas@bgs.ac.uk

Keywords: fractal dimension, topology, fracture pattern, fold-thrust

Highlights

- A new method for characterising fractures in fold-and-thrust belt structural settings with complex fracture networks
- Fractal dimensions and topological features are combined to characterise fractures enabling distinction of structural domains
- Reduced time taken for data collection compared to traditional fracture sampling techniques
- Fore-thrusts and back-thrusts have higher fractal dimensions than pop-up structures
- Fore-thrusts have fewer longer fractures
- Back-thrusts have higher densities of interconnected fractures

Abstract

Fractures in limestones of the Palaeocene Lockhart Formation in the hanging wall of the Himalayan Main Boundary Thrust north of Islamabad are examined, and the data analysed using a combination of topology and fractal dimension to characterise fracture patterns and relate them to structural domains. Neither technique alone allows the recognition of the structural domains. However, when considered together for all the fractures within an area, fore-thrusts, pop-ups and back-thrusts can be recognised. The fractures are considered together, as the characteristics of the individual structural domains are characterised by the cumulative effect of all the different fractures. Fore- and back-thrusts have higher fractal dimensions than pop-up structures. The highest fractal dimensions of both types of thrusts occur immediately adjacent to and decrease away from the central pop-up structure. Topologically, fore-thrust domains have fewer fractures and fracture intersections (nodes), with a longer mean fracture trace length; back-thrust domains contain more nodes (hence also more tips, lines, and branches) resulting in higher fracture densities. Pop-up structure domains are characterised by a low fracture intensity. Using the combined analysis of both the topology and fractal dimension, we show that the fracture pattern characteristics are predictable, when related to the different structural settings identified within fold and thrust of the Lockhart Formation.

1. Introduction

Fracturing of a rock mass is the mechanical response to an applied stress (Ramsey, 1967; Brown, 2008), with the extent and characteristics of the resultant fracture network controlled by the mechanical properties of the rock mass and variations in the stress field. Understanding the properties and characteristics of the resultant fracture network is essential in many aspects of applied geoscience, from determining the stability of an excavation (Hoek and Brown, 1980) to identifying fluid pathways and storage volumes for minerals (Cox, 2005) or hydrocarbons (Aydin, 2000).

Fracture systems are defined as geometrical arrays of linked and often interacting fractures within a rock mass (Rouleau and Gale, 1986; Odling *et al.*, 1999). Fracture systems have attracted much scientific attention and numerous methods have been proposed to characterise them, ranging from analysis of their kinematic behaviour, through shared and/or discrete geometry, to tectonic setting, as concisely and instructively summarised by Peacock and Sanderson (2018).

The geometric arrangements of fractures in a rock volume are typically viewed as either discrete objects in space (Barros-Galvis, *et al.*, 2015; Welch *et al.*, 2015), or topologically, that is to say, 'in relation to one another' (Long and Witherspoon, 1985; Laubach *et al.*, 2018), and/or in direct relation to causative mechanisms.

Studies that consider the spatial distribution of fractures as discrete objects provide valuable insights into the relationships between fractures and lithological characteristics of the fractured rock mass. For example, the spacing of fractures commonly varies with lithology or, more correctly, with differences in the mechanical properties of the lithology, such that competent lithologies display more widely-spaced fractures, for a given stress, compared to their less competent counterparts (Pollard and Fletcher, 2005; Ortega *et al.,* 2010; Hooker *et al*, 2013). Fracture spacing also varies with bed thickness (Ladeira and Price, 1981) with thicker beds containing more widely-spaced fractures than their thinner equivalents, for a given stress. In folded strata, differences in the geometry of fracture patterns are related to variations in competence and bed thickness and a response to the complex strain distribution in fold systems. This results in a broad array of geometrical fracture characteristics associated with ductile/brittle-ductile fold deformation features (Cosgrove, 2015; Ferrill *et al.,* 2016).

By contrast, topological analysis of a fracture network characterises the connectivity of the constitutive fractures in that network, rather than the inherent properties of the individual fractures (Sanderson *et al.*, 2019). This approach has provided an improved understanding of the overall behaviour of the physical properties of the rock mass under consideration, particularly in terms of its strength, porosity, and permeability (Sanderson and Nixon, 2015).

Approaches to fracture characterisation that establish a causative relationship between a particular fracture system and the mechanism responsible for its formation require observations that can indicate a temporal link between a fracture network and the proposed process (Long, *et al.*, 1996). Examples include studies of how fracture systems of different ages (established by geochemistry) link together to control mineralisation within Archean orogenic gold (Dziggel *et al.*, 2007) or recognition of mining-induced fractures and pre-existing geological discontinuities and how they interact to produce the rock mass around a mining stope (Grodner, 1999).

The task of relating a fracture system to a specific process is particularly challenging for rocks that have been subjected to multiple deformational events. For example, in fold-and-thrust belts deformation results from a combination of burial, changes in fluid pressure and composition, folding, thrusting, uplift and exhumation (Engelder *et al.*, 1985; English and Laubach, 2017). The distribution of fractures variously reflects the different failure responses to stresses of these events due to variations in mechanical properties of the rock mass (Wennberg *et al.*, 2006), that themselves evolve through time (Laubach *et al.*, 2009). Progressive folding can also result in multiple generations of opening-mode fractures (Cosgrove, 2015). Consequently, polyphase deformation in fold-and-thrust belts typically results in complex, sequential overlays of fracture networks with such high abundances and intricate patterns that they are not readily described by simple fold-fault-fracture geometries (Cosgrove, 2015), or by one-dimensional descriptors (Watkins *et al*., 2015; Laubach *et al.*, 2018). Fractures formed at the same time can have different orientations and mineral compositions and conversely fractures formed at different times can have the same orientations or mineralisation. To properly quantify the effects of the fracture networks on the rock mass, the whole fracture system must be considered rather than apparently discrete fracture sets in a fracture network (Peacock *et al.*, 2018).

Here we present a novel approach to the challenges involved in developing an informative, and potentially predictive, characterisation of highly fractured rock. The individual constituent fracture types within the fracture system are not separated for analysis, but rather we consider how the cumulative effects can be used to discriminate different structural domains. This approach integrates discrete topological and spatial methods for characterising fractures and fracture networks by employing fractal dimension to provide a spatial context of the distribution of the constituent fractures, and then combining those data with analyses of the observed topological relationships and interconnectivity of the fracture networks. The approach provides a more robust assessment and analysis of the fractures observed within the rock mass and their characteristics than can be achieved from application of either method in isolation. As we consider all the topological and fractal data together, all the interactions between fractures, and their effects upon the characteristics of the rock mass are defined. Moreover, this approach dramatically reduces the time taken for data collection compared to traditional fracture sampling techniques and provides large amounts of unbiased data representative of fracture network characteristics over a wide range of fracture structural domains.

We apply this technique to examine the occurrence and distribution of fracturing in well-exposed in Palaeocene limestones within the frontal thrust sheets associated with the Main Boundary Thrust (MBT) of the Himalayan fold and thrust belt (Tariq *et al.*, 2017; Dasti *et al.*, 2018), in a region approximately 10 km north of Islamabad, NW Pakistan (Figure 1 and Figure

2). Here, in a single stratigraphic unit (the Lockhart Limestone) a complex sequence of fractures can be studied across fore-thrusts, back-thrusts, and pop-up structures that all occur above, and immediately to the north of the MBT. We recognise that there are multiple generations of fractures in the study area, but as the geomechanical properties of the rock mass must be the result of all fractures combined, we contend that it is important to consider all fractures collectively to understand differences in the cumulative distribution of fracture sets related to specific structures. Restricting the structural analysis to a single stratigraphic unit removes variation in fracture characteristics related to lithology.

2. Regional Geological Setting

The geology of the study area in the Potwar Basin of northern Pakistan, immediately adjacent to the capital city of Islamabad (**Error! Reference source not found.**), is dominated by sedimentary deposits and structural features associated with the collision of the Indian and Eurasian plates during the Himalayan Orogeny (Acharyya and Saha, 2018). Continual southwards-directed and décollement-related thrusting of the crust of the Indian Plate resulted in a variety of high-level fold and fault structures in the hanging walls of the major thrusts that crop out in northern Pakistan (Yeats and Hussain, 1987; Pivnik and Wells, 1996; Burg *et al.*, 2005). As one of these major thrusts, the MBT is a regional-scale structure that demarcates the southern limit of the Peshawar-Hazara Basin, transporting a Mesozoic-Tertiary marine sequence of the Indo-Pakistan Plate south-eastwards over the syn-tectonic molasse of the Murree Formation sediments (Iqbal and Bannert, 1998; Ghani *et al.*, 2018).

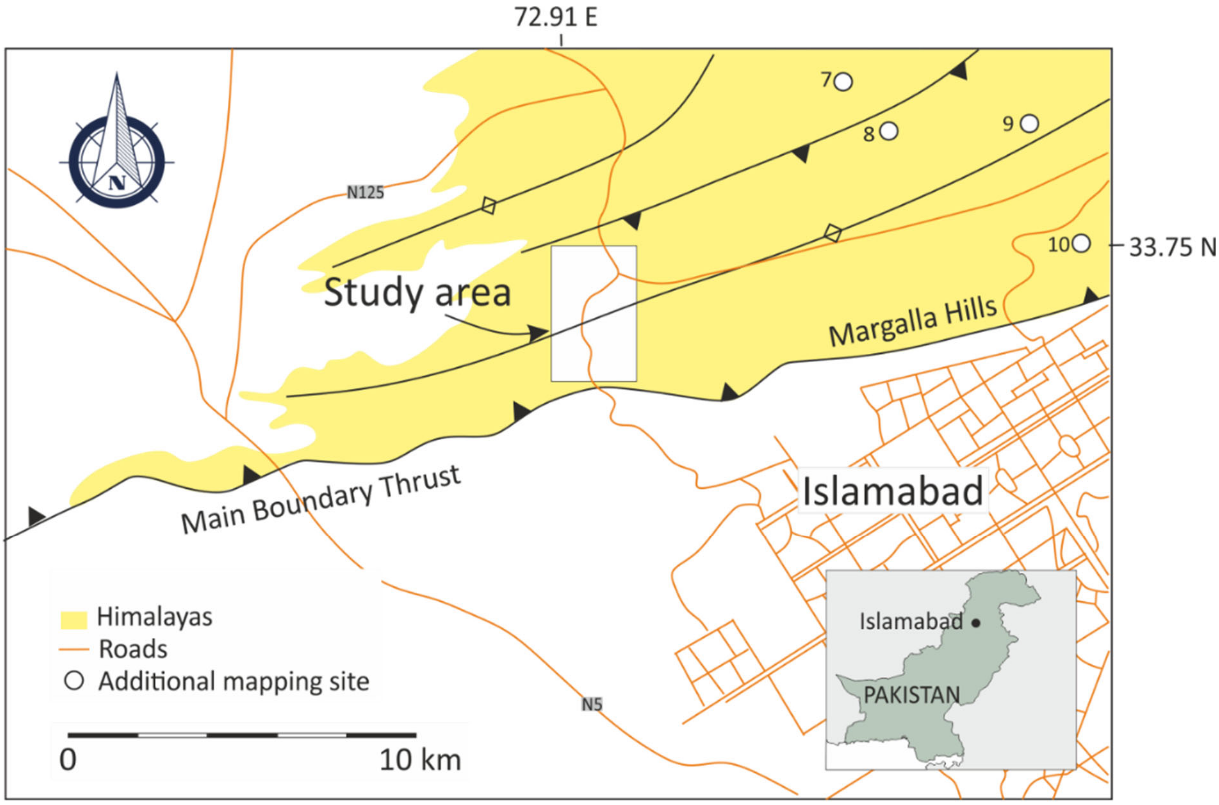

Figure 1: Location of the principal study area and additional mapping sites (7 to 10) in the foothills of the Himalayas north of Islamabad, Pakistan. Several tectonic structures are developed in the hanging wall strata of the Main Boundary Thrust and they form the focus of this study.

Sediments ranging from Precambrian evaporite, through Permian and Triassic siltstone-dominated sequences to successions of Jurassic sandstone, shale and limestone are present locally, but do not crop out in the study area and hence are not considered further. All analyses were undertaken on limestone units of the Palaeocene Lockhart Formation (Figure 2) which were deposited unconformably over Cretaceous fluvial and marine sediments on the northern leading edge of the Indian Plate during the closure of the Palaeo-Tethys Ocean (Chatterjee and Bajpal, 2016). Strata of the Lockhart Formation comprise a series of stacked foraminiferal–algal build-ups intercalated with argillaceous siltstone and mudstone, all deposited in cyclical units on a low-energy shelfal carbonate ramp, with the sediments recording many shallowing and shoaling events from open marine to inner ramp conditions (Hanif *et al.*, 2014). The limestone units of the formation generally comprise lime-mudstone, argillaceous wackestone and, more rarely, packstone, all with little or no primary matrix porosity.

Strata of the Lockhart Formation are overlain by siltstone and limestone of the late Palaeocene Patala Formation and the Eocene Nammal and Margalla Hill formations. This is a result of continued conformable deposition on a low-energy, shallow-marine shelf that shallows to a lagoonal and supratidal setting by the end of the Eocene Epoch (Hanif *et al.*, 2014; Wandrey *et al.*, 2004).

Eocene strata are overlain unconformably across the whole of the Potwar Basin by Miocene fluvial sediments (Wandrey *et al.*, 2004) that record deposition of post-initial collision Himalayan molasse. Pleistocene and Holocene superficial deposits complete the depositional record and consist of windblown silt and sand, along with alluvial gravel adjacent to the active thrust scarps (Robert *et al.*, 1997).

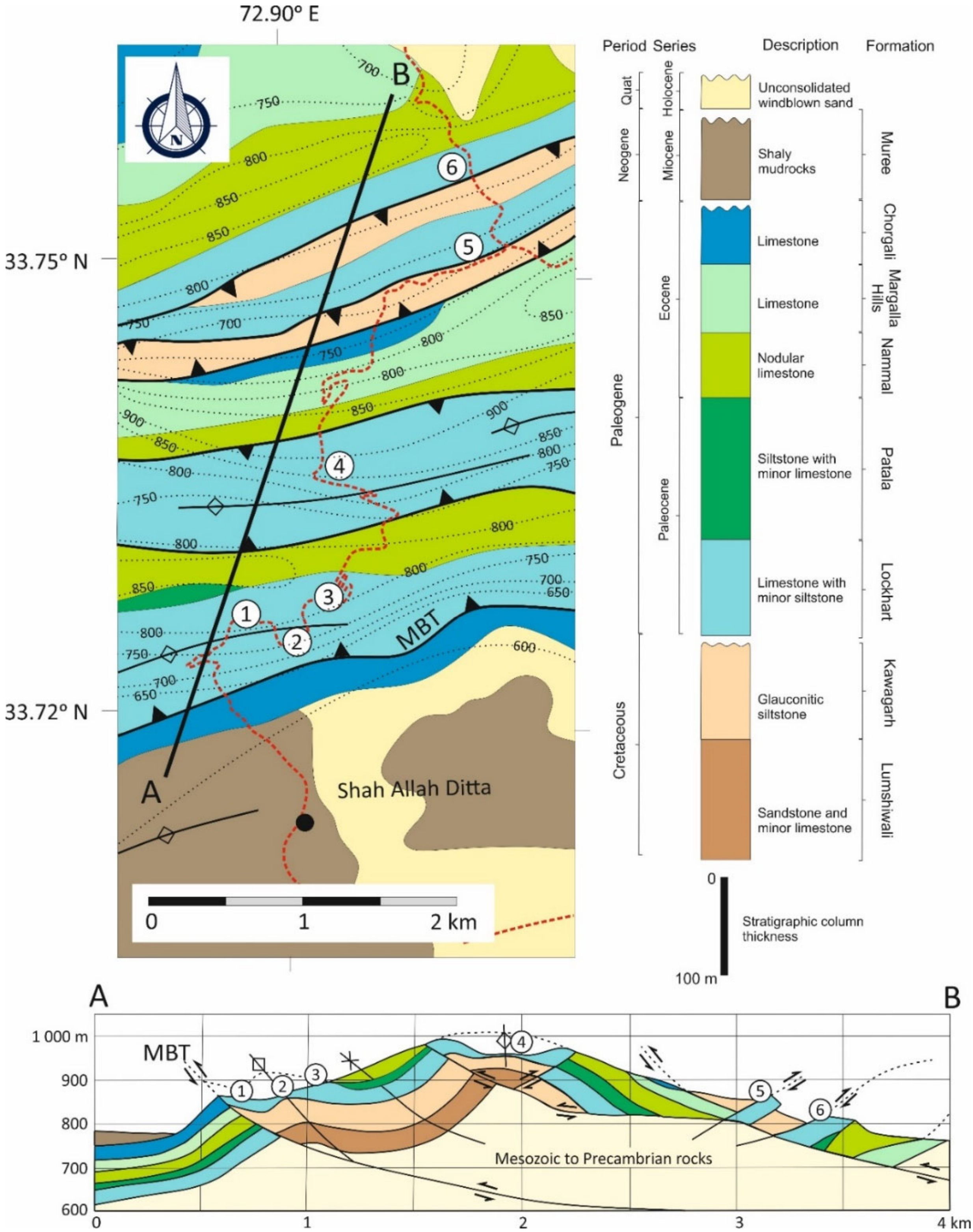

Figure 2: Geology of the study area with the positions of the primary study sites in the transect line indicated by numbers. Surface elevations in metres above mean sea level are indicated by dotted lines on the map. Dotted lines on the cross-section are projections of the strata. MBT = Main Boundary

Thrust. This dataset is augmented by further data from four sites 15 km northeast along strike (Figure 1). Geological map modified after Ali (2014) to conform with field mapping undertaken in this study. Interpretations of deeper levels on the cross section are from Williams *et al.* (1997). Vertical exaggeration: x2.

3. Methodology

3.1 Nomenclature and site selection

The dataset used to test the method described in this study comprises field measurements of fractures in the limestone-dominated strata of the Lockhart Formation associated with the MBT in northern Pakistan. These strata display a spectrum of brittle geomechanical behaviours across a range of scales, within units of limestone with very low porosity, interbedded with units of argillaceous siltstone and mudstone. By restricting collection of fracture data to locations within the well-exposed Palaeocene Lockhart Formation only, we remove the effects of lithological variation upon the dataset. Furthermore, all of the fractures characterised are located within the hanging wall of the MBT (Robert *et al.*, 1997; Iqbal and Bannert, 1998), and all have been subjected to the same regional tectonic stress field. For clarity, fracture nomenclature and terminology adopted in this study are summarised in Table 1.

Table 1: Nomenclature and descriptive terminology as applied in this study.

Term	Meaning
Fracture	Sub-planar, brittle discontinuity separating the mechanical properties of a rock. It is very narrow in width relative to the other two dimensions. The term considers extension fractures (joints and veins) as well as shear fractures with negligible displacement sub-parallel to the fracture (Peacock *et al.*, 2018).

Fracture set and fracture system	A fracture set is a subsection of a fracture system within a rock mass with similar properties (Peacock *et al.*, 2018). Properties could include orientation, mineralisation, or genetic origin. The cumulative characteristics of a fracture system are formed by the interaction of different fracture sets that need to be considered together to define the rock mass characteristic
Rock mass	A matrix consisting of intact rock and associated fractures. The properties of a rock mass are a product of the intact rock and of the fractures (Bieniawski, 1973; Barton, *et al.*, 1974; Laubscher, 1977).
Nodes	Terminations and intersections of fractures used in the topological analysis of the fracture data (Sanderson and Nixon, 2015).
Measurement circle and box	A one metre diameter circle drawn on a scaled digital photograph of rock exposure and used to define the measurement area for topological analysis. A one metre wide square box is centred on the circle and used to generate the box-counting grids for determination of the fractal dimension.
Fractal dimension	A quantification of the self-similarity or scale invariance of a fracture network. There and numerous methods to quantify the fractal dimension but in this study, we employ the box-counting method (see Figure 6 and Figure 7).
Topology	Quantification of the arrangement of fractures and how they are connected, from which it is possible to derive the physical characteristics of fractures, including fracture density, fracture intensity, mean

	fracture trace length, and the number of fracture tips, lines, and branches.

Six principal sites were chosen to examine the differences in fracture characteristics related to successive major structures (fore-thrust, pop-up, and back-thrust) of the Himalayan fold and thrust belt (Figure 2). To increase the geographical extent of the dataset, further data were acquired from four sites located along strike (and approximately 15 km northeast) of the major structural features observed in the primary transect line (Table 2), thereby expanding the significance of the analysed results and their interpretation. All sites lie within the Margalla Hills, approximately 10 km north of Islamabad, Pakistan (Figure 1). The brittle limestone and interbedded subordinate mudstone of the Lockhart Formation observed at all these sites are highly deformed and fractured. The study area is, as a whole, contained within a series of south-verging thrusts, north-verging back-thrusts, and associated folds and pop-up structures, all located within the hanging wall of the MBT (Tariq *et al.*, 2017; Dasti *et al.*, 2018).

Table 2: Locations and structural styles of the sites examined in the Lockhart Formation. Sites 7 to 10 are additional supporting sites located along strike from the main transect line formed from sites 1 to 6 (see Figure 1 and Figure 2).

Site	Latitude (° N)	Longitude (° E)	Structure
1	33.724	72.917	Fore-thrust with trailing anticline
2	33.723	72.921	Fore-thrust with trailing anticline
3	33.726	72.926	Fore-thrust with trailing syncline
4	33.733	72.922	Pop-up anticline
5	33.745	72.934	Back-thrust
6	33.750	72.933	Back-thrust
7	33.799	73.074	Back-thrust
8	33.781	73.063	Back-thrust
9	33.778	73.079	Pop-up anticline
10	33.779	73.060	Fore-thrust

Outcrop-scale geological data captured from each site (Table 2 and Figure 2) include the lithologies present, bedding thickness, and the types of sedimentary features preserved. All exert a significant role in defining rock mass behaviour and will thus influence the structures developed during deformation (Ortega *et al.*, 2010; Hooker *et al.*, 2013; Procter and Sanderson, 2018).

Individual fractures have lateral extents on the scale of centimetres to millimetres and vary in type and orientation within a small area (Figure 3); characterising each individual fracture is therefore inappropriate at the outcrop scale in these strata. Moreover, the wide range of fracture strikes at any one measurement site means that the one-dimensional scanline technique (Guerriero *et al.*, 2010) will have a strong bias as fractures that are sub-parallel to the scanline are less likely to be intersected by it. For such inherently two-dimensional patterns, techniques of rectangular or circular window mapping (Mauldon *et al.*, 2001; Watkins *et al.*, 2015) are preferable. A significant advantage of these techniques is the opportunity to derive topological information from these observations (Mauldon *et al.*, 2001; Sanderson and Nixon, 2015).

Fractures of similar orientation, thickness, and type, which may represent a fracture set, vary in abundance across the study sites, and may not necessarily correspond to the same structural event (Laubach *et al.*, 2010). The presence of earlier fractures will affect subsequent deformation, as high compressive stresses are required for the fracture tip to propagate through a pre-existing discontinuity (Renshaw and Pollard, 1994) and the original fracture orientation and aperture distribution are rarely preserved in later fractures (Long *et al.*, 1996). Because of this, it is not always possible to recognise a fracture set based on their orientation and hence relative ages of the fractures. To correctly define the rock mass characteristics, we measure the characteristics of all of the fractures together.

At each sampling location a circle of 1 m in diameter was marked onto the outcrop and captured through a minimum of four high-resolution digital photographs taken to cover a 1 m by 1 m square centred upon the measurement circle. Several circular windows were mapped at each sampling site, on surfaces oriented both parallel to and perpendicular to bedding, and on surfaces created by road-excavations at oblique angles to bedding (Table 3). Analyses of the fracture characteristics at each of the sampling sites are based on the combined data of all the circular windows, thereby reducing orientation bias.

Table 3: Number of circular windows and their orientations relative to bedding at the measurement sites along the transect.

Site	Mapping points			
	Parallel	Perpendicular	Oblique	Total
1	3	2	1	6
2	1	1	2	4
3	-	2	-	2
4	1	1	-	2
5	1	-	2	3
6	1	1	1	3
Total	7	7	6	20

3.1 Determination of topological characteristics

Topology describes the way in which constituent parts of a system are arranged, interrelated, and connected. The arrangement of components within a geometrical system – in this case, a fracture network – can be defined in terms of topology, and an analysis of that arrangement can provide critical information on network pathways. For example, a high number of cross-cutting fractures suggests interlinked networks with continuous pathways between them. The topological characteristics of a fracture network can be determined at any scale (Sanderson and Nixon, 2015).

The types of intersections (termed 'nodes') between fracture traces present within the measurement circles at each of the sites in this study were characterised. The types of nodes are defined as follows (Mauldon *et al.,* 2001; Sanderson and Nixon, 2015), and are identified in all subsequent diagrams by the colour and shape indicated in parenthesis (Figure 3):

- X nodes (red star) – intersections of fracture traces that cross each other and continue,
- Y nodes (green triangles) – termination of one fracture trace against another fracture trace,
- I nodes (blue circles) – termination of a fracture trace within the rock mass contained within in the circle,
- E nodes (yellow squares) - intersections of fracture traces with the edge of the circle where the traces continue out with the circle.

The nodes separate fracture traces into segments known as branches. X nodes have four branches, Y nodes have three, and I and E nodes have one branch each (Figure 4).

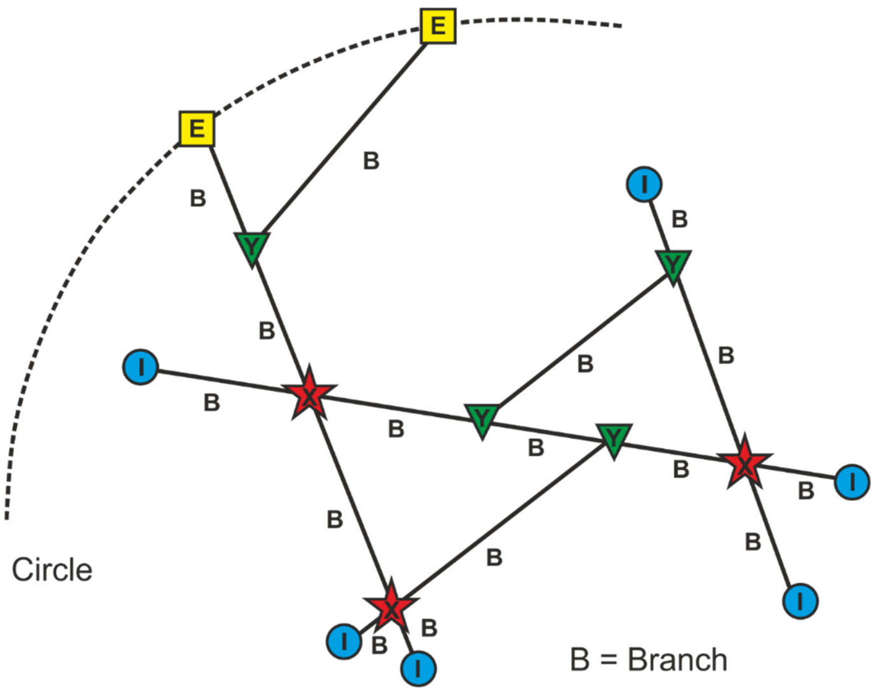

Figure 4: Node types of intersecting fracture traces as defined by Sanderson and Nixon (2015). Fracture branches are labelled “B”. Every X (red star) node has four branches, every Y (green triangle) node has three branches and every I (blue circle) or E (yellow square) node has one branch.

By counting the quantity and types of the nodes in the various measurement circles we were able to determine the topological characteristics of the fracture network from the following the methodology of Sanderson and Nixon, (2015). The number of fracture trace terminations within the circle is the sum of the number of I-nodes (N_I) and the number of Y-nodes (N_Y). The number of fracture traces contained within the circle (N_L) is half of the number of terminations as each trace is terminated at each end by either an I- or Y-node. Consequently:

$$N_L = \frac{1}{2}(N_I + N_Y)$$

As each fracture branch (Figure 4) has two nodes, with an I-node forming one termination of a branch, a Y-node terminating three branches and an X-node terminating four branches, the number of branches (N_B) may be calculated from:

$$N_B = \frac{1}{2}(N_I + 3N_Y + 4N_X)$$

The number of connections per line is a measure of fracture connectivity (F_c) that describes the degree of interlinking of the fractures. It is defined by:

$$F_c = \frac{4(\mathrm{N_X} + \mathrm{N_Y})}{\mathrm{N_Y} + \mathrm{N_I}}$$

The parameters of fracture intensity, density and mean trace length are derived from the nodes with the following relationships (Mauldon *et al.*, 2001):

- Fracture Intensity, (F_I) is a comparative measure of the number of edge-nodes (N_E), within a measurement circle (of radius r) and is defined by:

$$F_I = \frac{N_E}{4r}$$

- Fracture Density (F_D) represents the number of fractures per unit area. As a fracture is terminated inside a measurement circle of radius r by either a Y or an I node, the density is given by:
-

$$F_D = (N_Y + N_I)/2\pi r^2$$

- The Mean Trace Length (MTL) provides an estimate of the average fracture trace length as it considers the number of fractures that are contained within the measurement circle of radius r and the number that transect it. It is derived from multiplying Intensity by area and dividing by number of lines:

$$MTL = \frac{\frac{N_E}{N_Y + N_I}\pi r}{2}$$

Topological analysis of all the fractures was undertaken in a measurement circle and all the nodes, including those formed between different fracture sets, were accounted for at the same time to define the true topological characteristics. Table 4 and Figure 5 demonstrate that not considering all the nodes in a single measurement will result in an under-accounting of the intersecting “x” and “y” nodes, an over-accounting of the number of “i" nodes and an under-estimate of the total number of nodes. This will affect the calculation of the topological characteristics.

Table 4: Number of nodes measured when considering all fracture sets together in a single measurement compared to summing the number of nodes of individual fracture sets from Site 3. The number of “e” is the same, “x” and “y” nodes are more common in the former and “i" in the latter. This indicates a greater number of intersections are present when all fractures are considered together. The ratio of nodes changes, altering the topological characteristics.

		Node type	e	x	y	i	all
Single measurement		Unmineralised	19	48	71	97	235
		Mineralised	23	33	58	202	316
		Total	42	81	129	299	551
Set 1	> 25 cm	Unmineralised	8	0	6	14	28
		Mineralised	7	3	9	36	55
		Total	15	3	15	50	83
Set 2		Unmineralised	10	2	6	58	76

	10 - 25 cm	Mineralised	4	3	10	51	68
		Total	14	5	16	109	144
Set 3	< 10 cm	Unmineralised	1	17	17	110	145
		Mineralised	12	4	25	97	138
		Total	13	21	42	207	283
Sum of sets		Unmineralised	19	19	29	182	249
		Mineralised	23	10	44	184	261
		Total	42	29	73	366	510

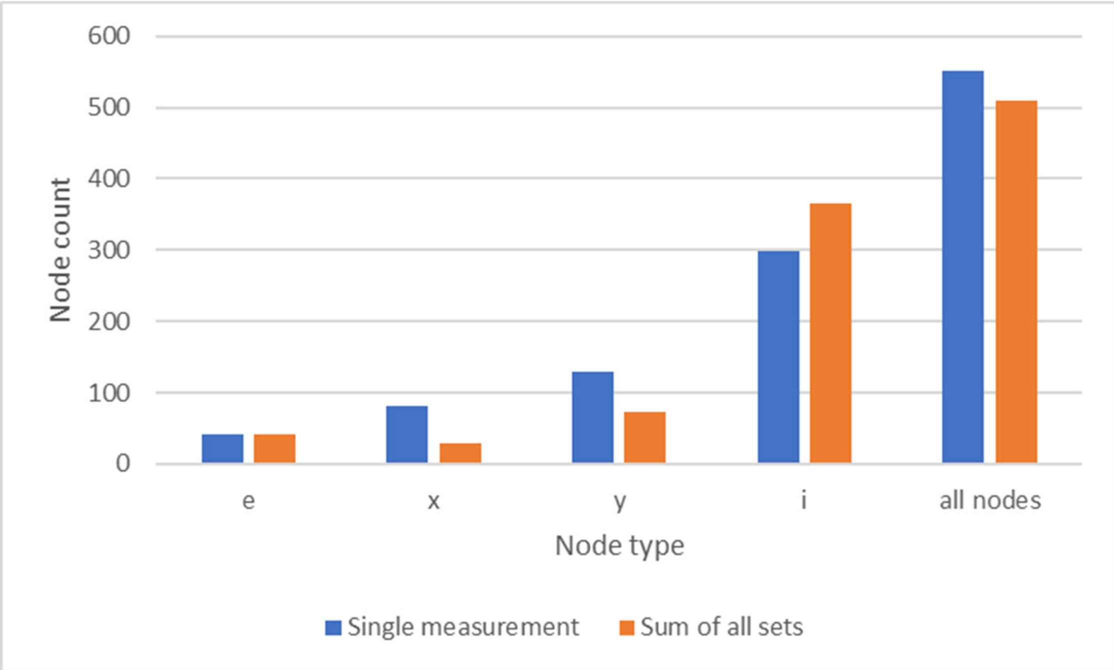

Figure 5: Number of different types of nodes present at Site 3, according to measurement type. The ratios and total number of nodes is different if all fractures are considered in a single measurement.

3.2 Determination of fractal dimensions

Complex scale-independent shapes can be quantified relative to the spatial dimension (1D, 2D or 3D) in which they are observed. The intermediate dimensions are referred to as fractal dimensions and have values between the dimensions of the objects and the dimensions in which the objects are observed. In this work, fractal dimensions are between one (the dimension of a fracture line) and two (the dimensions of the measurement surface).

In this study, fractal dimensions are calculated using a scale-independent box-counting method as defined by Mandelbrot (1967) and employed by many authors to characterise fractures (e.g. Cahn, 1989; Kagan, 1991; Odling, 1994; Berntson and Stoll, 1997; Libicki and Ben-Zion, 2005; Zhang, 2020). Other methods for the calculation of fractal dimensions, such as the probability-density (Nykamp, 2020) or pair correlation functions (Satoh, 2003), which compare the number of points closer together than a specific distance with the total number of points, may also be employed. Importantly, the fractal dimension calculated using the box counting and the pair correlation methods have the same average values (Mou and Wang, 2016). The point analysis methods are typically utilised where there is uncertainty in the validity of the much simpler and more widely recognised box-counting methods.

1 m-by-1 m measurement squares with grids of different box-sizes are placed over the 1 m diameter topology measurement circles, and the number of boxes containing fracture traces counted (Figure 5). Following the methodology of Walsh and Watterson (1993), the measurement squares do not extend beyond the edge of the fractured portion of the rock. Although the box counting squares do not cover the same areas as the 1 m diameter topological measurement circles, the squares are centred on the circles and the same size squares are analysed for the different box sizes, thus providing comparable data.

The slope of the log-log plot of the inverse of the box length versus the number of boxes containing fractures at each box size (Figure 7) is defined as the box-counting fractal dimension (Foroutan-pour *et al.*, 1999). Trend lines with correlation coefficients of at least 0.98 are generally considered to be representative of the fractal dimension (Liang *et al.*, 2012; Zhihui *et al.*, 2013). A slightly lower minimum correlation coefficient of 0.95 was considered acceptable in this study, given the comparatively smaller scale range of box sizes used (Figure 7).

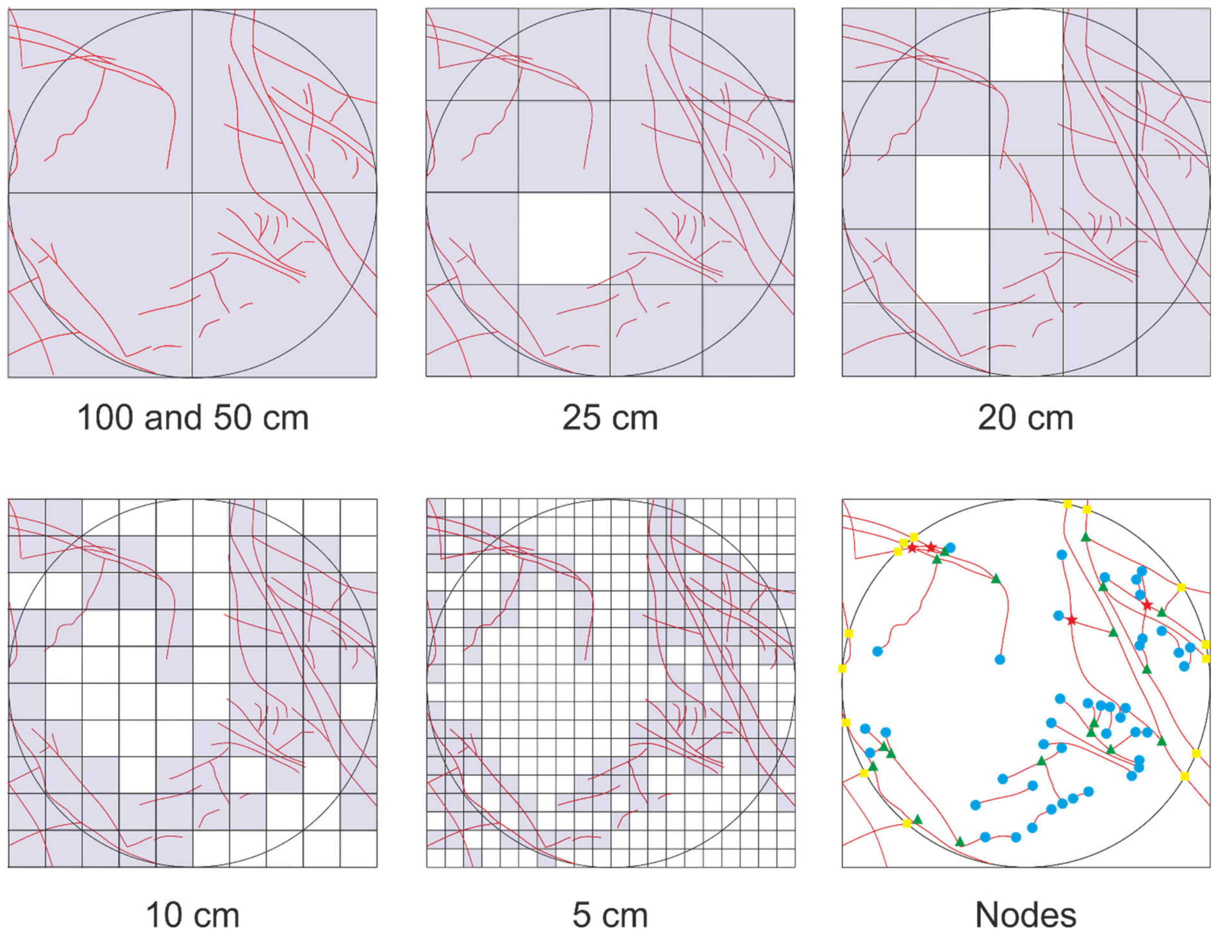

Figure 6: Box counting grids (grid size indicated beneath each circle) are placed over a measurement circle and only boxes that contain a fracture trace are summed (shaded boxes) and used to determine the box-counting fractal dimension. The associated topological node data are also shown (see Figure 4 for description of node symbol colours and shapes). Nodes outside of the circle are not considered in the topological analysis.

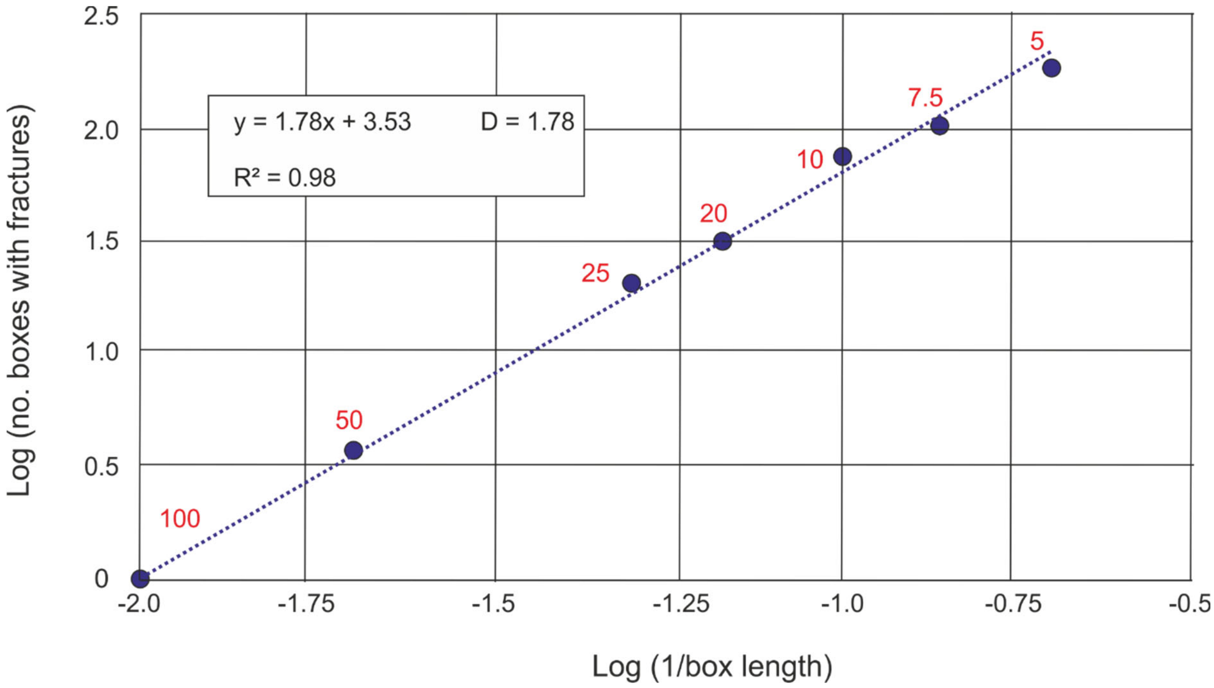

Figure 7: Log-log plot of data from Site 4. The gradient of the best-fit trend-line is the fractal dimension of these data. Red numbers indicate box side length in centimetres.

If the box sizes are too large or too small then the gradient of the trend-line may form a plateau at either end of the plot (Walsh and Watterson, 1993). No significant changes in the gradient of the trend-lines were observed for all sites in this study. Thus, the box size distribution of between 5 cm and 1 m is considered appropriate for these lithologies in this context.

4. Fracture characteristics of the study sites

Four principal fracture types are observed in the limestone rocks examined in this study (Figure 3):

(a) Explosive, hydro-fracture-type calcite-filled veins without any dominant orientation trends,

(b) unmineralised clusters of sub-parallel fractures,

(c) clay- or gouge-filled shear fractures typically oriented parallel to bedding or with multiple cross-cutting relationships close to folds and thrusts,

(d) sub-parallel, calcite-filled veins that increase in abundance with proximity to thrusts of large displacement.

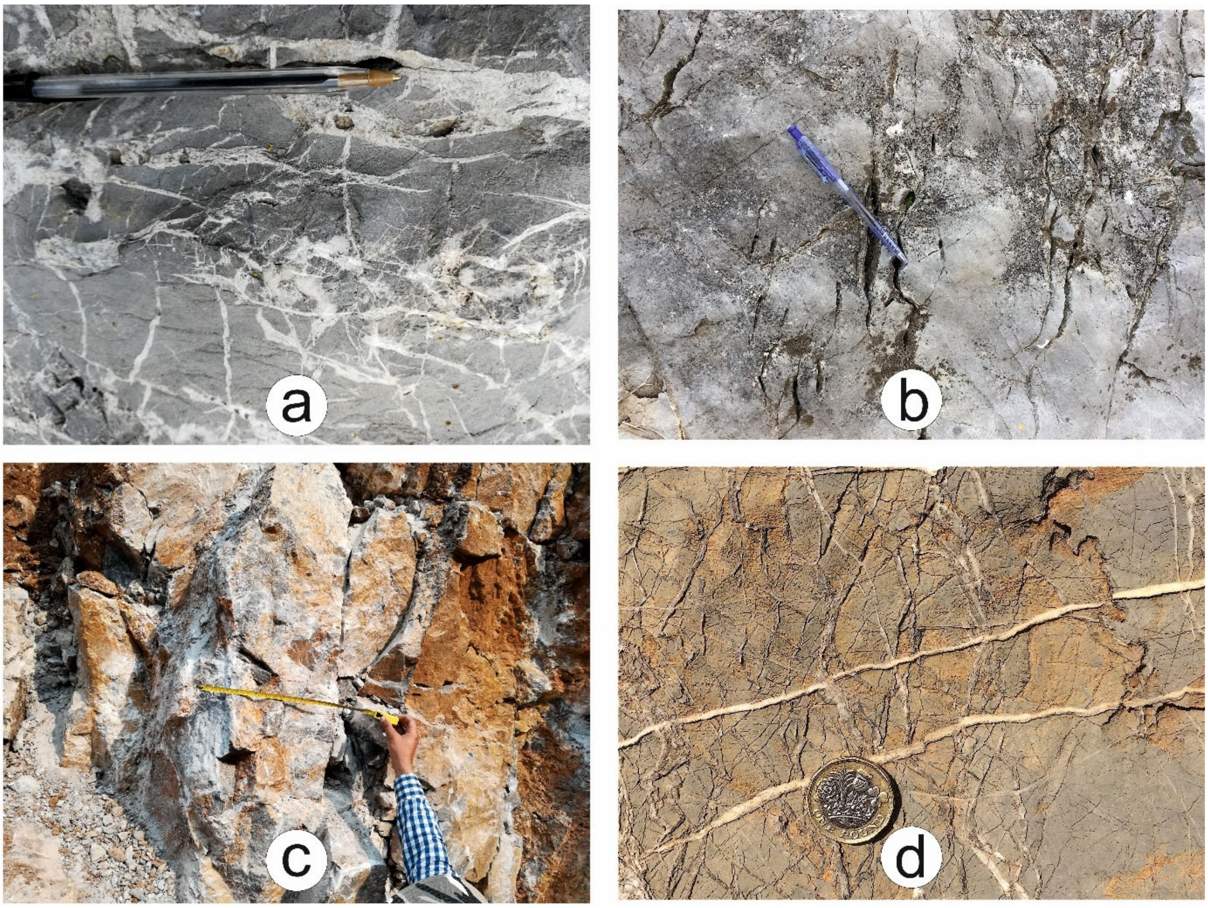

Figure 3: Principal fracture types of this study. (a) explosive hydro-fractures, (b) unmineralised clusters of sub-parallel extension fractures, (c) clay / gouge filled shear fractures, (d) sub-parallel calcite-filled veins. These principal fracture types can occur individually or combine as pairs, or as fracture systems of three or four different principal types.

These principal fracture types are present at all sites studied and occur individually or combine as pairs, or as fracture systems of three or four different principal types.

4.1. Characteristics of total fracture sets

Site 1 is located 500 m north of the Himalayan MBT (Figure 2). The site consists of tightly folded limestone units of the Lockhart Formation (Figure 8). A highly deformed shaly siltstone unit, with centimetre-thick, structurally induced laminations, forms a decollement surface over the tightly folded 0.4 m thick limestone beds.

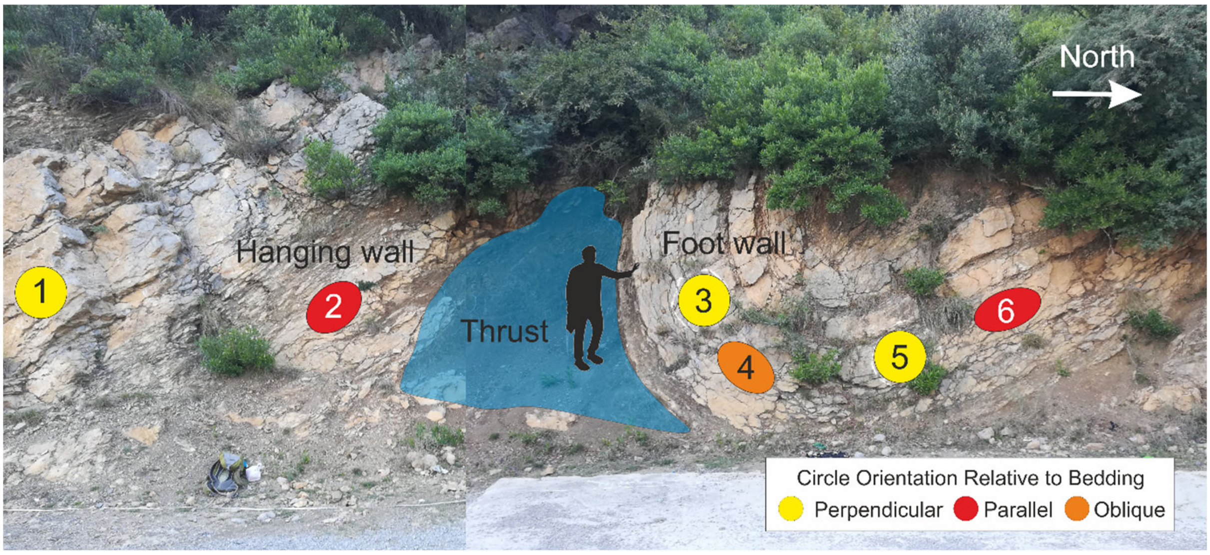

Figure 8: Site 1 - tightly folded limestone units (circles 3, 4, 5 and 6) and siltstone with limestone (circles 1 and 2) overthrust northwards. The measurement circles, with their associated box-counting squares, are in different orientations relative to bedding (see also Table 3).

Although there is little difference in the total number of nodes measured in each of six circles placed across the structure at Site 1 (Figure 8) the proportions of different types of nodes vary between circles relative to their orientation and distance from the thrust as displayed in Appendix 1 which also details these characteristics for all the mapping sites. In the hanging wall of the thrust at Site 1 (Circle 1), there are very few X nodes formed from cross-cutting fracture traces, but equal numbers of Y and I nodes formed from fracture terminations. Towards the thrust (Circle 2) E, X and Y nodes increase in proportion relative to I nodes. In the footwall of the thrust (Circles 3 to 6) the measurement circles have similar numbers of nodes to each other and further from the thrust, the fractures display a progressive increase in connectivity but decrease in fracture density. The fractal dimension is 1.88 at this site.

Site 2 is only 400 m away from Site 1 (Figure 2), but the structural geology is significantly different. Interbedded limestone and shaly siltstone of the Lockhart Formation are folded into a tight, upright anticline with a wavelength of approximately 20 m and an amplitude of approximately 60 m. The sedimentary succession consists of beds of argillaceous limestone, each on average 20 cm thick, combining to form 60 cm thick units bounded by centimetre-thick laminated mudstone units, younging into alternating packstone and dark-grey wackestone beds, each approximately 10 cm thick. The strongly laminated wackestone has a high fracture intensity, but a low number of branches due to bedding-parallel failure along the thin shaly units. The lack of cross-cutting fractures reduces the connectivity of fracture network. Due to the interlayered nature of the limestone and mudstone lithologies, the site displays a wide range in fractal dimensions of between 1.72 and 1.92. Although some of the thinner limestone units have fractal dimensions of greater than 1.8, most of the rock mass deformation has deformed through shearing along bedding planes, reducing the fractal dimension. This fracture pattern also results in a lower fracture density as much of the applied stress is accommodated by shearing, rather than by the development of additional fractures.

Site 3 is located in a succession of 1.5 m thick limestone beds of the Lockhart Formation. The presence of a single, large, through-going fracture results in a high degree of connectivity, and a high fractal dimension of 1.97 (virtually a 2D plane). In contrast to this, numerous fractures that are less than 1 mm wide have high intensity but low connectivity. The abundant small fractures also cause a low overall mean trace length for the site.

Site 4 is situated in a relatively undeformed pop-up anticline bounded between sets of fore-thrusts and back-thrusts (Figure 2). The limestone units of the Lockhart Formation at this site consist of packstone beds – approximately 30 cm thick – dipping 14 degrees towards the south-southwest. The topological characteristics and the fractal dimension of the bedding-plane parallel fractures closely match those of the bedding-perpendicular fractures.

The broad, easily accessible back-thrust thrust surface formed on an approximately 1 m thick limestone bed at Site 5 has prominent calcite veins developed both parallel to and perpendicularly to the thrust on the exposed surface. The dominant thrust-parallel calcite-filled fractures and thicker thrust-perpendicular fractures (that are also therefore parallel to the fault propagation fold axis) are more widely spaced and the mean trace length is approximately half that of the sites in the fore-thrust. Small, millimetre-thick, calcite-filled fractures with short trace lengths of up to 5 cm are common throughout in a variety of different orientations resulting in a large number of nodes. The different topological and fractal details of these elements are combined to define the general rock mass behaviour of the back-thrust. The observed fractures have the highest number of branches (264) and highest fracture intensity (20.7) and density (37.9) of all the measurement sites. They are also characterised by a shorter mean trace length (14) than Sites 1,2,3, and 10 in the fore-thrust. Due to the high degree of fracturing, the site has a high fractal dimension of 1.93.

Site 6 is the most northerly mapping location and hence furthest from the MBT. This site is dominated by limestone beds approximately 1 m thick, with irregular centimetre-thick argillaceous siltstone partings that are highly sheared. Several classic thrust structures are evident, including relatively undeformed footwall strata immediately beneath the thrust plane.

The thrust fault and the associated fault propagation fold zone at Site 6 are both highly fractured. The footwall to the thrust comprises a foraminiferal packstone that is typical of the upper stratigraphy of the Lockhart Formation, which is only weakly deformed with discontinuous, variably oriented, thin (1 mm or less) calcite-filled fractures. Thrust-parallel fractures are present, none of which are mineralised, and there are very few brittle tensile fractures associated with the thrust-related folding. However, the rock mass within the fault propagation fold area is highly fractured, iron oxide-rich bedding-parallel thrust surfaces and steeply dipping fault propagation fold fracture planes. The limestone fragments between these fractures all contain abundant scattered, millimetre-wide, calcite-filled fractures.

The average fractal dimension of circular measurement windows from the thrust footwall at Site 6 is 1.56. In the thrust hanging wall, the bedding- and thrust-parallel fractures are better connected than the thin calcite-cemented tensile fractures that display the highest number of tips, lines and branches, and a high dimension of 1.92. When the measurements of the folded hanging wall and thrust-plane itself are included, the dimension increases from 1.56 to 1.80, which reflects the variability that occurs when considering different parts of a geological structure. This variation accounts for the overlap between the groupings based on the larger scale descriptions of a geological structure, such as "fore-thrust", when individual portions of a specific structure display different fractal properties. Despite there being a high number of fracture intersections in the footwall (524 in total), there are very few edge intersections (only 4%) and cross-cutting fractures (7%). Moreover, 55% of the fractures do not terminate against another fracture.

The Lockhart Formation is well exposed in the back-thrust at both Site 7 and Site 8 along strike from sites 5 and 6. The rocks of these sites consist of highly fractured metre-thick, grey foraminiferal packstone that is less intensely fractured than the other back-thrust sites resulting in lower fractal dimensions (1.82 and 1.83).

The flat dipping centimetre thick mudstone beds of Site 9, exposed in a river valley that runs perpendicular to the regional strike, have few fractures and the lowest fractal dimension (1.76). This is due to a combination of the stratigraphy (thinly bedded strata) and structural setting (in a pop-up zone), with the limited applied stresses being released by bedding parallel shearing.

At Site 10, the Lockhart Formation has been folded into an anticline with a wavelength of approximately 10 m and an amplitude of 25 m. Flexural flow has been facilitated by centimetre-thick mudstone-limestone layers, reducing the number of fractures on the interbedded light-grey coloured 0.5 m thick limestone beds in this fore-thrust setting.

5. Analysis of fractal and topological characteristics

In order to understand how the fracture networks vary spatially across the fold and thrust belt, the measured topological parameters and fractal dimensions are cross-correlated. The data employed to undertake this analysis are presented in Appendix 1.

Sites 1 to 6 are described in detail above as they provide an ideally oriented distribution of successive structural domains from a fore-thrust, through a pop-up to a back-thrust and the associated fracture patterns. Additional data from four supplementary sites located along strike from the main transect (Figure 1) have been included to confirm the characterisation of the fracture pattern in different structural domains by using this combination of the topological and fractal characteristics (see Figure 9).

When the average fractal dimension and the average total number of nodes of each type in the fracture network at each of the sites are examined, characteristic values are apparent. The fore-thrust and pop-up structures have lower total numbers of nodes than the back-thrusts, and the pop-up has the lowest fractal dimension whilst the fractal dimension is higher in in both the fore-thrust and back-thrust (Figure 9).

By plotting, not just the average, but also the range of these values, cross-plot correlations between fractal dimensions and total number of nodes may be drawn (Figure 10) showing the trends in the changes in the characteristics of the fracture system.

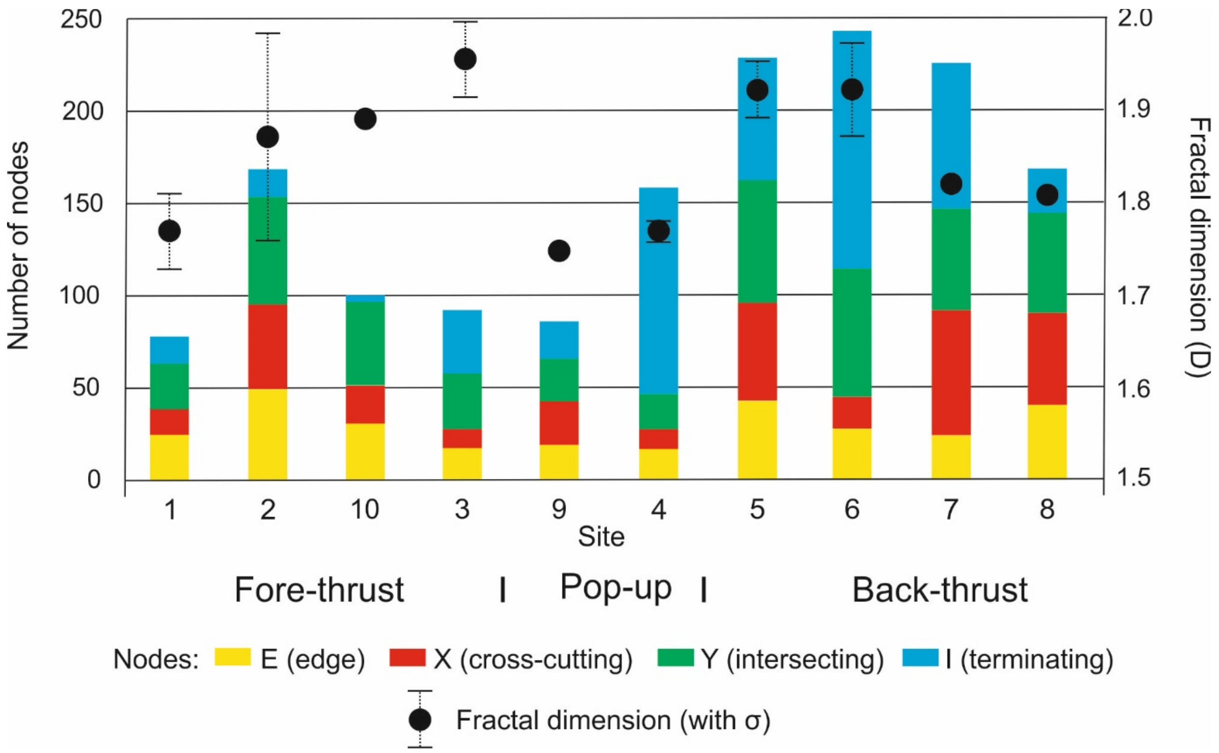

Figure 9: Average number of nodes and fractal dimensions at each site, grouped according to structural domain. Note the greater number of nodes and proportion of I nodes at sites in the back-thrust structural domain. The fractal dimension is lowest in sites within the pop-up structural domain.

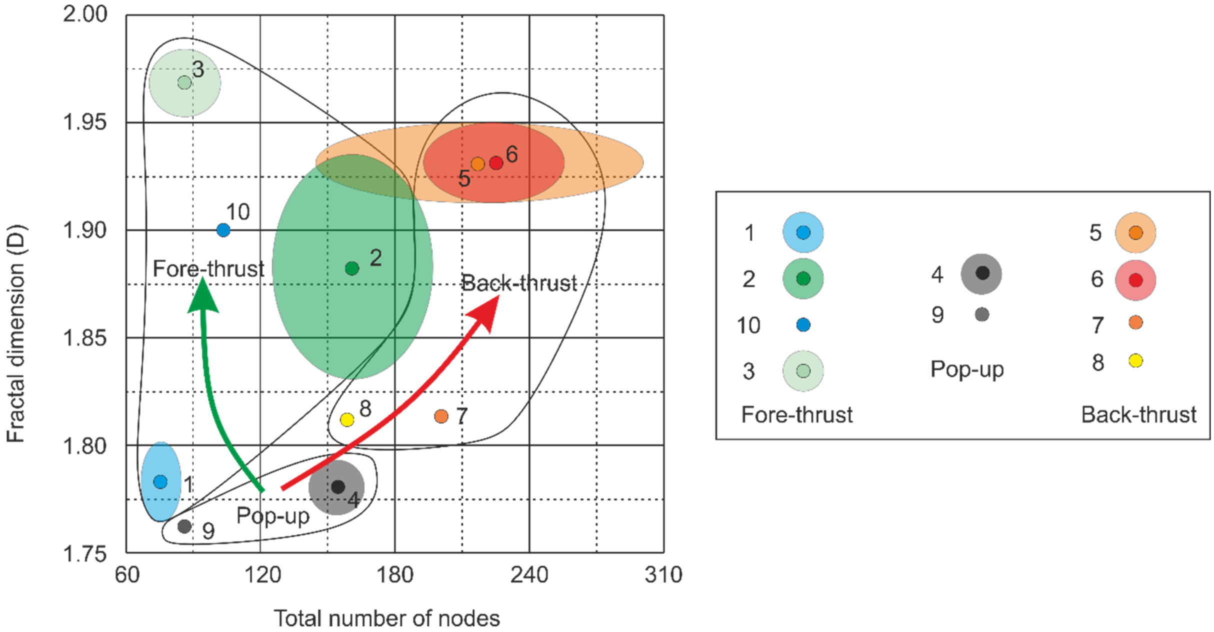

Figure 10: Average total number of nodes vs. average fractal dimension of the various sites in the different structural domains. The average values of datasets from each site are indicated by small bold circles and the standard deviations of the datasets are indicated by the more transparent ellipses of the same colour. Bold circles with no ellipses represent sites with a single measurement circle. Trends in the number of nodes and fractal dimension from the pop-up to the fore-thrust and back-thrusts are shown by the green and red arrows, respectively.

Figure 11 and Figure 12 show the variations in the fractal dimensions and topology of the different structural domains. The longer mean trace length in the fore-thrust and greater number of branches and higher fracture density in the back-thrust are evident on these graphs, as is the low fractal dimension of the pop-up structure.

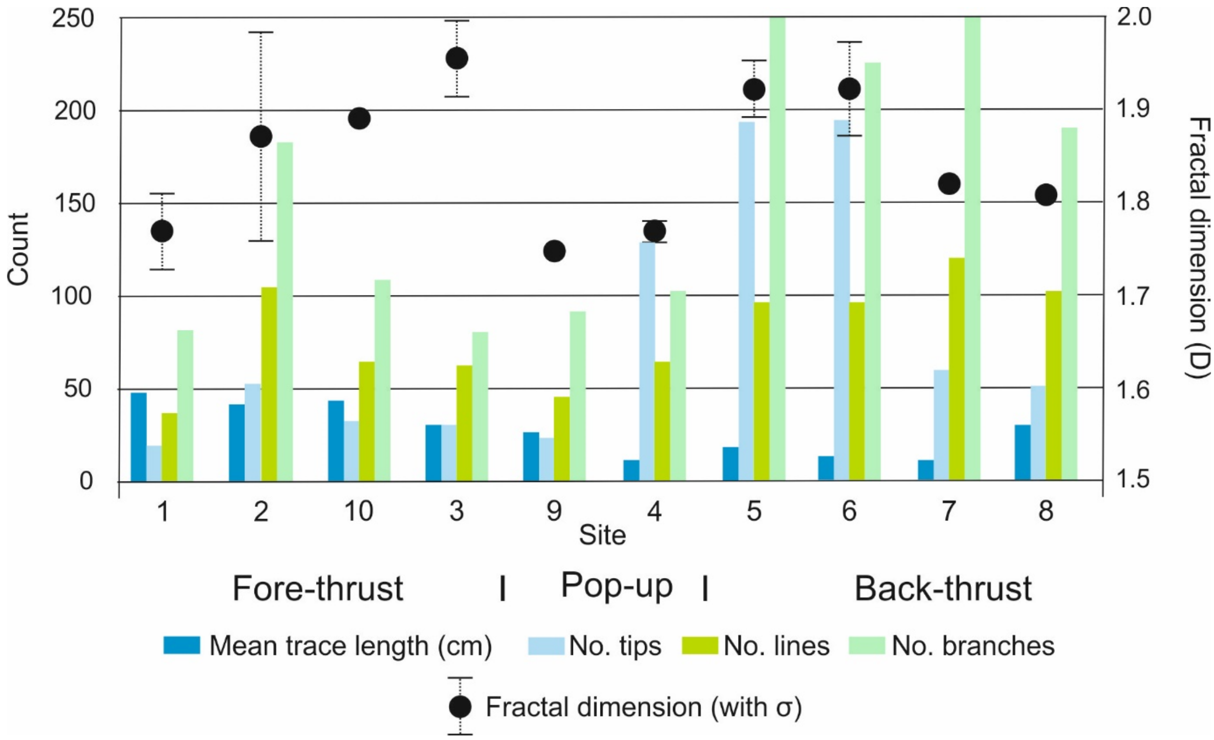

Figure 11: Fracture characteristics (mean trace length, number of tips, lines, and branches) derived from the analysis of topological data and fractal dimensions for different sites.

The differences in the fractal dimension and fracture characteristics derived from the topology of the different structural domains are best shown by comparing them against each other graphically. The basic topological parameters of the number of tips, lines and branches are inputs into the fracture density, connectivity, intensity, and mean trace length which are plotted against the fractal dimensions to illustrate these relationships with the fractal dimension for the different structural settings in this study (Figure 13).

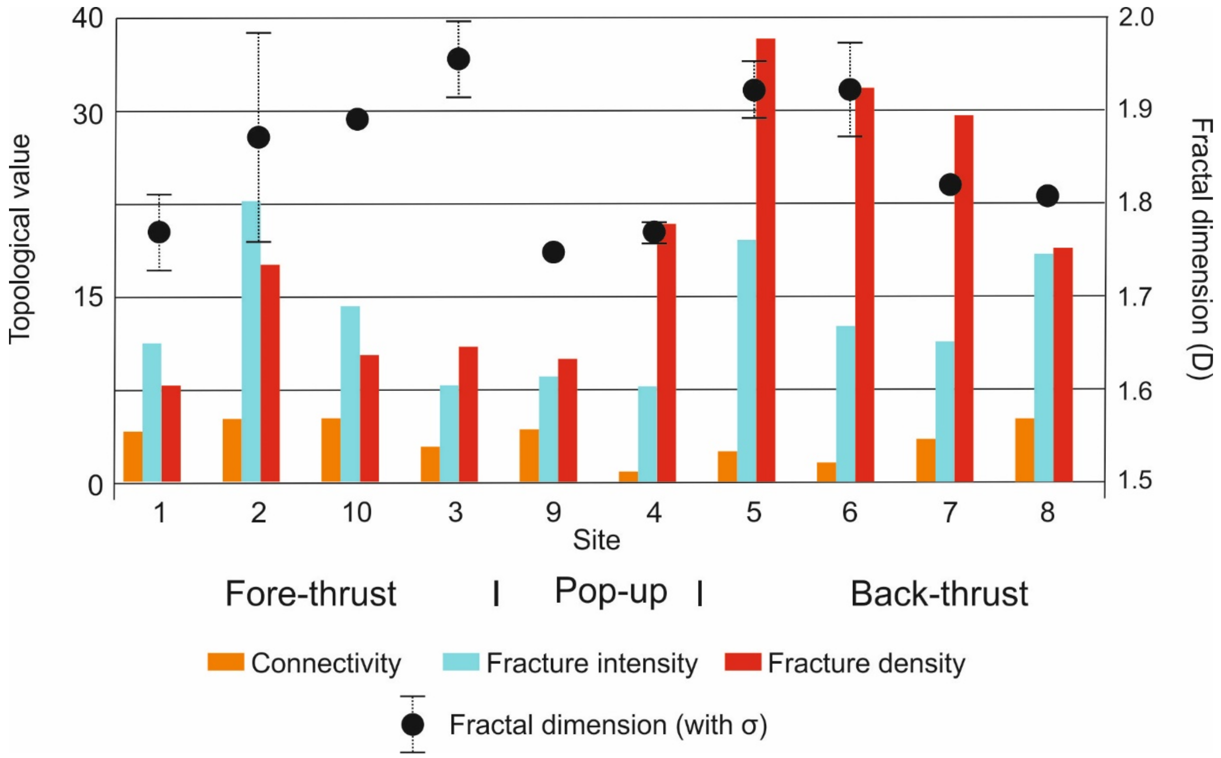

Figure 12: Fracture characteristics (connectivity, fracture intensity and fracture density) derived from the analysis of topological data and fractal dimensions for different sites.

When the average and range of topologically derived fracture characteristics and fractal dimensions are considered in different structural domains, distinct relationships are apparent (Figure 13 and Table 5). Fore-thrusts are characterised by fewer, longer, well-connected fractures and back-thrusts contain a higher number of fractures with more tips, lines, and branches but these are not as well interconnected. The highest fractal dimensions of the fore-thrust and back-thrust are immediately adjacent to the pop-up zone (Figures 10 and 11). As the pop-up zone(sites 4 and 9) between the fore-thrust and back-thrust has a lower fractal dimension and also displays the lowest connectivity, fracture intensity and mean trace length indicating that it is the least disturbed structural domain and can thus be used as the starting point from which the characteristics of the fore- and back-thrusts evolve and are superimposed (Figure 13).

The higher fracture density and lower connectivity and mean trace length apparent in the topological data of the back-thrusts (Sites 5, 6, 7 and 8) is due to the predominance of small, shorter fractures. The fore-thrusts (Sites 1, 2, 3 and 10) display more, longer fractures with an associated increase in connectivity (Figure 13). Like the fractal dimension, the fracture intensity increases in both the fore-thrust and back-thrusts (Figure 13).

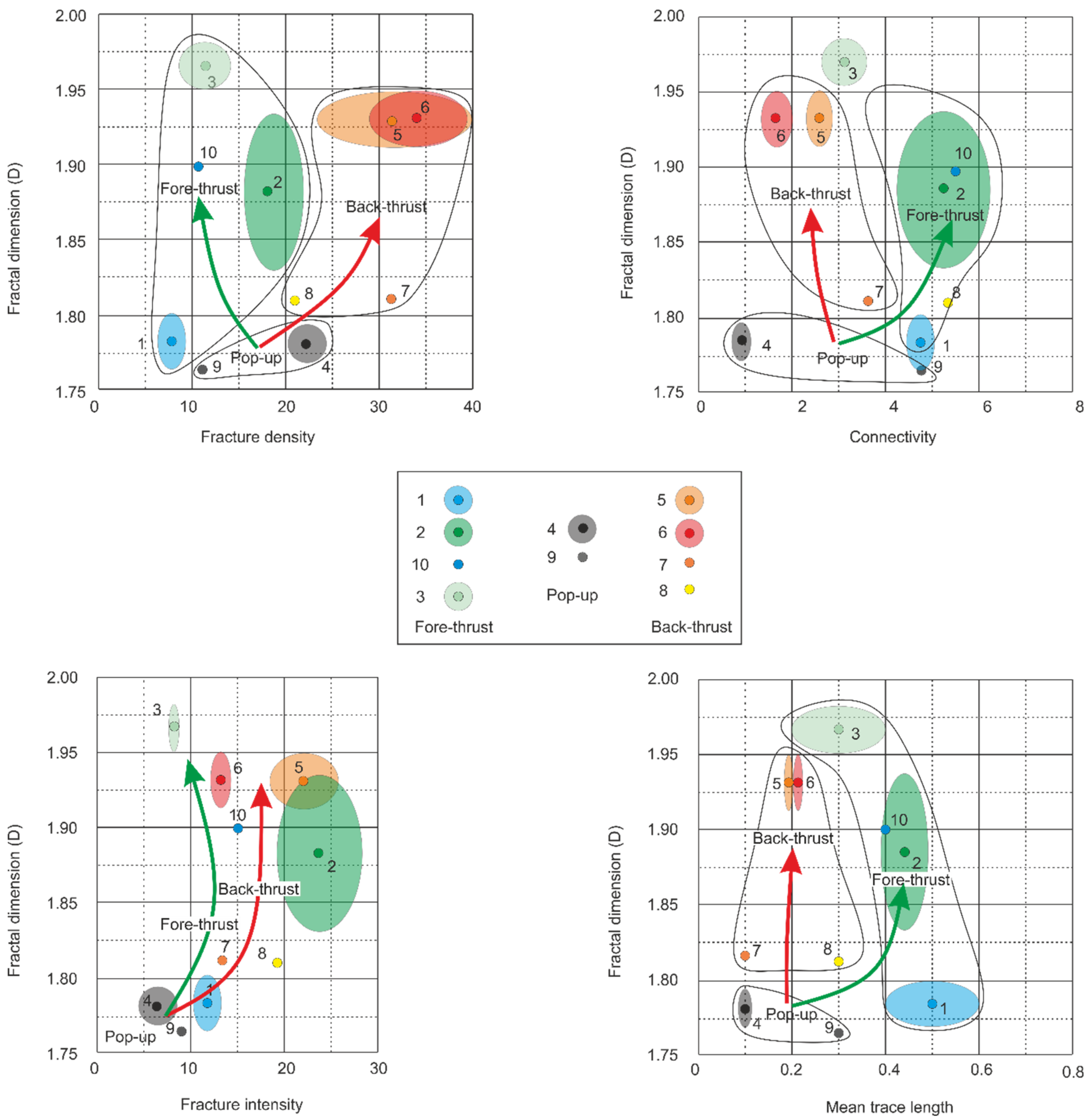

Figure 13: Fractal dimension (D) compared to fracture characteristics derived from topological analysis of data from different structural domains.

Average values of datasets from each site are indicated by bold circles and the standard deviations of the datasets are indicated by the more transparent ellipses of the same colour. Trends in the number of nodes and fractal dimension from the pop-up to the fore-thrust and back-thrusts are shown by the green and red arrows, respectively. There is good correlation between structural domain, fractal dimension and density, connectivity, and mean trace length. The correlation is poor when considering fracture intensity. It should be noted the reversed position of the fore-thrust and back-thrust locations within the graphs of fracture density as opposed to connectivity and mean trace length is due to the quantifiably different changes of these topological parameters in the two locations.

Table 5: Summary of topological and fractal characteristics. Back-thrusts have the highest average node count for each type, resulting in higher fracture density and number of tips, lines and branches compared to fore-thrusts but both domains have a similar range of fractal dimensions.

Structure	Characteristic
Fore-thrust	Fewer I nodes
	Lower total number of nodes
	Longer mean trace length
	D lower further from pop-up
Pop-up	Few E nodes
	Low fracture intensity
	Low number of lines
	Low number of tips
	Low number of branches
	Lowest D
Back-thrust	More nodes of all types
	Higher fracture density
	More tips
	More lines

	More branches
	D lower further from pop-up

As the fractal dimension is a measure of the distribution of a feature, in this case fractures, the similar range of values present in this work implies the rock mass deformed in a similar manner. However, the different fracture characteristics derived from the topological values indicate that the stress is accommodated differently in the fore-thrust and back-thrust setting. Intuitively, it is expected that fracture networks in the fore-thrust will have more extended fractures (greater mean trace length), due to extended periods of movement on the thrust sheets compared to back-thrust settings, where fracture networks are more irregular with higher fracture density, as a result of late-stage layer-parallel shortening.

The data presented here suggest that fore-thrusts are dominated by fewer but longer fractures that are the product of flexural flow, whereas the back-thrust appear to be dominated by tangential longitudinal failure. The low fractal dimension of the pop-up structure and the accompanying highest fractal dimension in the fore-thrusts and back-thrusts immediately adjacent to it shows that the fractal dimension can be used as an indicator of the proximity of change to a different structural domain.

6. Discussion

6.1. Significance of the cumulative effect of fractures

The methodology presented here is novel in that it quantifies the total rock mass of the limestone, including the fracture system within it, in a single set of measurements collected simultaneously on the fracture system. This approach not only enables efficient collection of data, dramatically reducing the time taken for data collection, but more importantly, it provides data that characterise the cumulative effects of the fractures, which may have resulted from multiple strength hardening or weakening processes, and their impact on the subsequent rock failure response (Laubach *et al.*, 2009; Corradetti *et al.,* 2015).

This is important, because from a geomechanical perspective, the behaviour of the rock mass is the sum of all its constituent inhomogeneities, including both lithological variation and all fracture sets. In each structural domain there is a general brittle failure pattern due to the stress-path that the rock mass has undergone (Everall and Sanislav, 2018). This will impact on subsequent fracture patterns. For example, it is necessary to carefully consider pre-existing fractures, possibly unrelated to folding, to build more realistic conceptual fold–fracture models (Lacombe *et al.*, 2011). This cumulative effect on the rock mass is especially relevant in successions when deformation is progressive, with successive fracture sets reflecting the rock response to cumulative strain. The formation of one fracture set controls the initiation or arrest of subsequent sets in an evolving stress regime by providing new stress concentrators and barriers for the deforming system. Consequently, it is not surprising that the occurrence of multiple sets of fractures is the rule rather than the exception in many fold and thrust belts (Salvini and Storti, 2001; Florez-Niño *et al.*, 2005; Iñigo *et al.*, 2012; Corradetti *et al.*, 2015; Burberry *et al.*, 2019). The combined effect of all the fracture systems therefore needs to be considered in a structural fracture analysis.

Fracture sets may form by sequential events and infilling, with earlier discontinuities acting as mechanical boundaries (Bai and Pollard, 2000). However, not all fractures of a particular set terminate on fractures of a set that was developed immediately prior to it, making it difficult to recognise fracture sets and hence define the mathematical laws that describe the distribution of each fracture set (Guerriro *et al.*, 2010). We do not attempt to discriminate between the different fractures, as characteristics such as composition, orientation or termination relationships & styles may not be unique to a set of fractures formed in response to one single deformation event Rather, by considering the numbers of all the different types nodes and the fractal dimension of all the fractures together, one can be confident that the all the various discontinuity constituents of the rock mass are included.

In the case of the data set from the Lockhart Formation limestone associated with the MBF, it is apparent that the standard deviation of the number of nodes of different fracture sets is significantly lower than the standard deviation of a group of all of the nodes of a fracture network. This provides quantitative evidence that only analysis of all fractures within the deformed rock volume is representative of the true complexity of the system and therefore mostly likely to be able to characterise specific structural domains.

6.2. Recognition of structural domains from fracture analysis

In our examination of the Lockhart Formation in the hanging wall of the MBF we demonstrate that the characteristics of the fracture systems in different structural domains can be recognised when all the fracture data are considered together. Fracture systems developed in both fore-thrusts and back-thrust settings have higher fractal dimensions than those in a pop-up structure. Hydro-fractures are present throughout all structural domains and do not vary in abundance relative to the structural regime. They probably represent slightly earlier phases of brittle deformation caused by initial thrusting and uplift events that promoted reductions in the confining stresses. Continued deformation allowed the other principal fracture types to develop with the longer calcite fractures and shear fractures forming close to thrusts. The unmineralised extension fractures and sometimes the shear fractures are associated with folds. As different fracture types formed contemporaneously, there is a complex interaction and overlap of all of the fracture types in this active fold and thrust belt which may not be easily resolved. Topologically, fracture networks in the fore-thrust setting are characterised by fewer nodes and a longer mean trace length, hence a lower density, but higher connectivity. By contrast, the topological characteristics of the back-thrust setting are dominated by more nodes producing a higher fracture density and lower mean trace length and higher intensity. The pop-up zone has an overall low fracture intensity.

By adopting an approach that considers both spatial and topological properties of fractures a relationship between fracture network parameters to structural domain is apparent. It is only by combining and comparing the two data types that the characterisation of structural styles become apparent. Moreover, the distinction of structural domains with fracture systems that are a result of the cumulative effects of multiple fracturing events is enhanced when all the constituent fracture sets that define the true characteristics of the rock mass are considered together.

7. Conclusions

A new approach of combining independently derived topological and fractal analyses of fracture networks has been developed to quantify the characteristics of highly deformed limestone in the Himalayan fold and thrust belt. This technique is employed to define the characteristics of complex, heterogenous fracturing in various structural settings within the hanging wall of the Himalayan Main Boundary Thrust north of Islamabad, Pakistan which has applicability to a wide variety of fracture networks in different tectonic settings. Moreover, this approach dramatically reduces the time taken for data collection and provides large amounts of unbiased data representative of fracture network characteristics.

By examining the topological characteristics and fractal dimension of all the fractures together it is possible to distinguish and quantify the fracture system of an area based on empirical evidence and use this to define specific structural domains. In general, the fracture systems developed in both fore-thrusts and back-thrust settings have higher fractal dimensions than those in a pop-up structure. The fractal dimension of both thrust types decreases away from the central pop-up zone. Topologically, the fracture networks in the fore-thrust setting have on average, fewer nodes and a longer mean trace length and hence a lower density, but higher connectivity. By contrast, the topological characteristics of the back-thrusts setting are dominated by more nodes producing a higher fracture density and lower mean trace length and higher intensity. The pop-up zone has a low fracture intensity.

This method represents a first attempt to relate fracture network parameters to structural style by adopting a combined approach that looks at both spatial and topological properties. It is only by combining and comparing the two data types that the characterisation of structural styles become apparent.

As a fracture system is not simply the sum of the sets of fractures, but also the interactions between them, we have developed a methodology that rapidly establishes the attributes of the overall rock mass. By combining the topological and fractal characteristics of the fractures into a single group, it avoids problems associated with the mis-identification and grouping of fractures that are not spatially or temporally related and thereby wholly representative of the rock mass in question. Through quantifying the cumulative characteristics of all the fractures in a single set of measurements, we can recognise different structural domains.

The utilisation of the methodology established in this study should be applicable to comparable lithologies in fold and thrust belts and a variety of different structural settings across a range of scales worldwide. This could be readily tested by using the same analytical techniques presented in this work, in either outcrop or subsurface settings.

8. Acknowledgements

This research is funded by Orient Petroleum Incorporated (OPI) and by the Acorn Fund at Keele University. OPI provided funding and logistical support for fieldwork in Pakistan. We gratefully acknowledge the assistance of OPI management and especially field geologists Muhammad Saleem and Israr Azfal and driver Khalid Nazar in this work. We thank John Walsh (Fault Analysis Group, University College Dublin) who kindly reviewed an earlier draft of the manuscript and helped greatly to clarify our thinking. We also thank the thorough reviewers that have ensured that the work is appropriate for publication.

9. References

Acharyya, S.K., Saha, P., 2018. Himalayan Paleogene Foreland Basin, its collision induced early volcanic history and failed rift initiation. Journal of Asian Earth Sciences 162, 3-12.

Ali, F. 2014. Tectonic Evolution of the Margalla Hills and a Part of the South Eastern Hazara Ranges, Pakistan. Unpublished Ph.D. dissertation, University of Peshawar, Pakistan.

Awdal, A., Healy, D., Alsop, G.I., 2016. Fracture patterns and petrophysical properties of carbonates undergoing regional folding: A case study from Kurdistan, N Iraq. Marine and Petroleum Geology 71, 149-167. http://dx.doi.org/10.1016/j.marpetgeo.2015.12.017.

Aydin, A., 2000. Fractures, faults, and hydrocarbon entrapment, migration, and flow. Marine and Petroleum Geology 17 (7), 797–814. https://doi.org/10.1016/s0264-8172(00)00020-9.

Bai, T., Pollard, D.D., 2000. Fracture spacing in layered rocks: a new explanation based on the stress transition. Journal of Structural Geology 22, 43-57.

Barton, N.R., Lien, R. and Lunde, J. 1974. Engineering classification of rock masses for the design of tunnel support. Rock Mech. 6(4), 189-239.

Barros-Galvis, N., Villaseñor, P., Samaniego, F., 2015. Analytical modelling and contradictions in limestone reservoirs: breccias, vugs, and fractures. Journal of Petroleum Engineering Article ID 895786. https://doi.org/10.1155/2015/895786.

Berntson, G., Stoll P., 1997. Correcting for finite spatial scales of self-similarity when calculating the fractal dimensions of real-world structures. Proc. R. Soc. B Biol. Sci. 264, 1531–1537. https://doi.org/10.1098/rspb.1997.0212.

Bieniawski, Z.T. 1973. Engineering classification of jointed rock masses. Transactions South African Institute of Civil Engineers 15, 335-344.

Burberry, C.M., Cannon, D.L., Cosgrove, J.W., Engelder, T., 2019. Fracture patterns associated with the evolution of the Teton anticline, Sawtooth Range, Montana, USA. In: Bond, C.E. and Lebit, H.D. (eds) Folding and Fracturing of Rocks: 50 Years of Research since the Seminal Textbook of J. G. Ramsay. Geological Society, London, Special Publications, 487. First published online 31 January 2019. https://doi.org/10. 1144/SP487.12.

Burg, J-P., Celerier, B., Chaudhry, N.M., Ghazanfar, M., Gnehm, F., Schnellmann, M., 2005. Fault analysis and paleostress evolution in large strain regions: methodological and geological discussion of the south eastern Himalayan fold-and-thrust belt in Pakistan. Journal of Asian Earth Sciences 24, 445–467.

Brown, E.T., 2008, Estimating the Mechanical Properties of Rock Masses. In: Potvin, Y. Carter, J., Dyskin, A., Jeffrey, R. (eds), Proceedings of the First Southern Hemisphere International Rock Mechanics Symposium, Australian Centre for Geomechanics, Perth. pp. 3-22. https://doi.org/10.36487/ACG_repo/808_16.

Cahn, R., 1989. Fractal dimension and fracture. Nature 338, 201 – 202. https://doi.org/10.1038/338201a0.

Chatterjee, S., Bajpil, S., 2016. India’s Northward Drift from Gondwana to Asia During the Late Cretaceous-Eocene. Proc Indian Nat. Sci. Acad. 82, 479-487.

Corradetti, A., Girundo, M., Tavani, S., Iannace, A., Parente, M. Mazzol, S., Strauss, C., Torrieri, S., Pirmez, C., Giorgioni, M. 2015. Analysis of Reservoir Scale Fracture Sets in Southern Italy's Carbonate Reservoir Analogues, Monte Faito, Sorrento Peninsula (Southern Italy). International Petroleum Technology Conference, Doha, Qatar, paper Number: IPTC-18433-MS. https://doi.org/10.2523/IPTC-18433-MS.

Cosgrove, J. W., 2015. The association of folds and fractures and the link between folding, fracturing and fluid flow during the evolution of a fold–thrust belt: a brief review. In: Richards, F. L., Richardson, N. J., Rippington, S. J., Wilson, R.W., Bond, C. E. (eds) Industrial Structural Geology: Principles, Techniques, and Integration. Geological Society, London, Special Publications, 421. http://dx.doi.org/10.1144/SP421.11.

Cox, S.F., 2005. Coupling between Deformation, Fluid Pressures, and Fluid Flow in Ore-Producing Hydrothermal Systems at Depth in the Crust. Economic Geology 100th Anniversary Volume 39-75.

Darcel, C., Bour, O., Davy, P., 2003. Stereological analysis of fractal fracture networks. Journal Geophysical Research 108 (B9) 2451, http://doi:10.1029/2002JB002091.

Dasti, N., Akram, S., Ahmad, I., Usman, M., 2018. Rock fractures characterisation in the Khairi Murat Range, Sub Himalayan Fold and Thrust Belt, North Pakistan. The Nucleus 55 (3) 115 – 127.

Dziggel, A., Otto, A., Kisters, A.F.M., Meyer, F.M., 2007. Tectono-metamorphic controls on gold mineralisation in the Barberton Greenstone Belt, South Africa: an example from the New Consort Gold Mine. In Van Kranendonk, M.J., Smithies, R.H., Bennet, V.C., (eds) Developments in Precambrian Geology (15). Elsevier B.V. https://doi:10.1016/S0166-2635(07)15058-1.

Engelder, T., 1985. Loading paths to joint propagation during a tectonic cycle: an example from the Appalachian Plateau, USA. Journal of Structural Geology 7(3-4), 459-476.

English, J.M., Laubach, S.E., 2017. Opening-mode fracture systems - Insights from recent fluid inclusion microthermometry studies of crack-seal fracture cements. In Turner, J.P., Healy, D., Hillis, R.R., and Welch, M., eds., Geomechanics and Geology: Geological Society, London, Special Publications 458, 257-272. https://doi:10.1144/SP458.1.

Everall, T.J., Sanislav, I.O., 2018. The influence of pre-existing deformation and alteration textures on rock strength, failure modes and shear strength parameters. Geosciences 8 1-23. https://doi.org/10.3390/geosciences804024.

Ferrill, D.A., Morris, A.P., Wigginton, S.S., Smart, K.J., McGinnis, R.N., Lehrmann, D., 2016. Deciphering thrust fault nucleation and propagation and the importance of footwall synclines. Journal of Structural Geology 85, 1-16. http://dx.doi.org/10.1016/j.jsg.2016.01.009.

Florez-Niño, J-M, Aydin, A., Mavko, G., Antonellini, M., Ayaviri, A. 2005. Fault and fracture systems in a fold and thrust belt: An example from Bolivia. AAPG Bulletin 89 (4) 471–493. https://doi.org/10.1306/11120404032.

Foroutan-pour, K., Dutilleul, P. Smith, D.J., 1999. Advances in the implementation of the box-counting method of fractal dimension estimation. Applied Mathematics and Computation 105 (2–3) 195-210.

Ghani, H., Zeilinger, G., Sobel, E.R., Heidarzadeh, G., 2018. Structural variation within the Himalayan fold and thrust belt: A case study from the Kohat-Potwar Fold Thrust Belt of Pakistan. Journal of Structural Geology 116, 34-46.

Grodner, M. 1999. Fracturing around a deep level gold mine preconditioned stope. Geotechnical and Geological Engineering 17, 291-304.

Guerriero V, Iannace, A, Mazzoli, S., Parente, M., Vitale, S., Giorgioni, M., 2010. Quantifying uncertainties in multi-scale studies of fractured reservoir analogues: Implemented statistical analysis of scan line data from carbonate rocks. Journal of Structural Geology 32, 1271-1278.

Halley, J. M., Hartley S., Kallimanis A. S., Kunin, W. E., Lennon, J. J., Sgardelis, S. P., 2004. Uses and abuses of fractal methodology in ecology. Ecology Letters 7, 254–271. https://doi:10.1111/j.1461-0248.2004.00568.x.

Hanif, M. Ali, F. Afridi, B.Z., 2014. Depositional environment of the Patala Formation in biostratigraphic and sequence stratigraphic context from Kali Dilli Section, Kala Chitta Range, Pakistan. Journal of Himalayan Earth Sciences 46(1) 55-65.

Hoek, E. and Brown, E.T., 1980. Underground Excavations in Rock. Institution of Mining and Metallurgy, London, 527 pp.

Hooker, J.N., Laubach, S.E., Marrett, R., 2013. Fracture-aperture sized frequency, spatial distribution, and growth processes in strata-bounded and non-strata-bounded fractures, Cambrian Mesón Group, NW Argentina. Journal of Structural Geology 54, 54-71.

Iñigo, J.F., Laubach, S.E., Hooker, J.N., 2012. Fracture abundance and patterns in the Subandean fold and thrust belt, Devonian Huamampampa Formation petroleum reservoirs and outcrops, Argentina, and Bolivia. Marine and Petroleum Geology 35(1), 201-218.

Iqbal, M., Bannert, D., 1998. Structural Observations of the Maragala Hills, Pakistan and the Nature of the Main Boundary Thrust: Pakistan Journal Hydrocarbon Research 10, 41-53.

Kagan, Y. Y., 1991. Fractal dimension of brittle fracture. Journal of Non-linear Science 1, 1–16.

Korvin, G., 1989. Fractured but not fractal: fragmentation of the Gulf of Suez basement. Pure and Applied Geophysics 131, 289-305.

Ladeira, F. L. and Price, N. J., 1981. Relationship between fracture spacing and bed thickness. Journal of Structural Geology 13, 179–83.

Laubach, S.E., Olson, J.E., Gross, M.R., 2009. Mechanical and fracture stratigraphy. AAPG Bulletin 93(11), 1413–1426. http://doi:10.1306/07270909094.

Laubach. S.E., Olson, J.E., Eichhubl, P., Fomel, S. Marrett, A., 2010. Natural Fractures from the Perspective of Diagenesis. Focus Article CSEG Recorder September 2010, 26-31.

Laubach, S.E., Lamarche, J., Gauthier, B.D.M., Dunne, W.M. Sanderson, D.J., 2018. Spatial arrangement of faults and opening-mode fractures. Journal of Structural Geology 108, 2-15. http://dx.doi.org/10.1016/j.jsg.2017.08.008.

Laubscher, D.H. 1977., Geomechanics classification of jointed rock masses -mining applications. Transactions of the Institute of Mining and Metallurgy 86, A1-8.

Liang, Z., Feng, Z., Guangxianga, X., 2012. Comparison of Fractal Dimension Calculation Methods for Channel Bed Profiles. Procedia Engineering 28, 252 – 257. https://doi:10.1016/j.proeng.2012.01.715.

Libicki, E. Ben-Zion, Y., 2005. Stochastic Branching Models of Fault Surfaces and Estimated Fractal Dimensions. Pure and Applied Geophysics 162 1077–1111.

Long, J.C., Witherspoon, P.A., 1985. The relationship of the degree of interconnection the permeability in fracture networks. Journal of Geophysical Research: Solid Earth 90(B4), 3087–3098.

Long, J.C.S., Aydin, A., Brown, S.R., Einstein, H.H., Hestir, K., Hsieh, P.A., Myer, L.R., Kenneth G. Nolte, D.L., Olsson, O.L., Paillet, F.L., Smith, J.L., Thomsen, L., 1996. Rock Fractures and Fluid Flow: Contemporary Understanding and Applications. The National Academies Press, Washington, DC. https://doi.org/10.17226/2309.

Mandelbrot B., 1967. How long is coast of Britain - statistical self-similarity and fractional dimension. Science 156, 636–638.

Mauldon, M., Dunne, W.M., Rohrbaugh, M.B. Jr., 2001. Circular scanlines and circular windows: new tools for characterising the geometry of fracture traces. Journal of Structural Geology 23, 247-258.

Mou, D., Wang, Z.W., 2016. Comparison of box counting and correlation dimension methods in well logging data analysis associate with the texture of volcanic rocks. Non-linear Processes Geophysics. Discussions. https://doi:10.5194/npg-2014-85.

Nykamp, D.Q., 2020. The idea of a probability distribution. Math Insight. http://mathinsight.org/probability_distribution_idea.

Odling, N.E., 1994. Natural Fracture Profiles, Fractal Dimension and Joint Roughness Coefficient. Rock Mech. Rock Eng. 27, 135-153. https://doi: 10.1007/bf01020307.

Odling, N. E., Gillespie, P., Bourgine, B., Castaing, C., Chiles, J. P., Christensen, N. P., Fillion, E., Genter, A., Olsen, C., Thrane, L., Trice, R. Aarseth, E., Walsh, J. J., Watterson, J.,1999. Variations in fracture system geometry and their implications for fluid flow in fractures hydrocarbon reservoirs. Petroleum Geoscience 5, 373-384. https://doi.org/10.1144/petgeo.5.4.373.

Ortega, O.J., Gale, J.F.W. Marrett, R., 2010. Quantifying diagenetic and stratigraphic controls on fracture intensity in platform carbonates: An example from the Sierra Madre Oriental, northeast Mexico. Journal of Structural Geology 32, 1943-1959.

Peacock, D.C.P., Sanderson, D.J., 2018. Structural analyses and fracture network characterisation: seven pillars of wisdom. Earth Science Reviews, 184 13-28.

Peacock, D.C.P., Sanderson, D.J., Rotevatn, A., 2018. Relationships between fractures. Journal of Structural Geology 106, 41-53.

Pivnik, D. A., Wells, N.A., 1996. The transition from Tethys to Himalayas as recorded in NW Pakistan: Geological Society of America Bulletin 108, 1295–1313.

Pollard, D. D., Fletcher, R. C., 2005. Fundamentals of Structural Geology. Cambridge University Press, Cambridge, 500 pp.

Procter, A., Sanderson, D.J., 2018. Spatial and layer-controlled variability in fracture networks. Journal of Structural Geology 108, 52-65.

Ramsay, J.G., 1967., The Folding and Fracturing of Rocks. McGraw-Hill, New York.

Redondo, J.M., Gonzalez-Nieto, P.L., Cano, J.L., Garzon, G.A., 2015. Mixing Efficiency across Rayleigh-Taylor and Richtmeyer-Meshkov Fronts. Open

Journal of Fluid Dynamics 5, 145-150. https://doi 10.4236/ojfd.2015.52017.

Renshaw, C.E., Pollard, D.D., 1994. Numerical simulation of fracture set formation: a fracture mechanics model consistent with experimental observations. Journal of Geophysical Research 99(18), 9359-9372.

Robert J. L., Kazmi, A.H. and Jan. M.Q., 1997. Geology and Tectonics of Pakistan. Graphic Publisher, Karachi, 554 pp.

Rouleau, A., Gale, J.E., 1985. Statistical characterization of the fracture system in the Stripa granite, Sweden. International Journal of Rock Mechanics and Mining Sciences & Geomechanics Abstracts 22(6), 353-367. https://doi.org/10.1016/0148-9062(85)90001-4

Salvini, F., Storti, F., 2001. The distribution of deformation in parallel fault-related folds with migrating axial surfaces: comparison between fault-propagation and fault-bend folding. Journal of Structural Geology 23 (1). 25-32. https://doi:10.1016/s0191-8141(00)00081-x.

Sanderson D.J., Nixon C.W., 2015. The use of topology in fracture network characterisation. Journal of Structural Geology 72, 55-66. http://dx.doi.org/10.1016/j.jsg.2015.01.005.

Sanderson, D.J., Peacock, D.C.P., Nixon, C.W., Rotevatn, A., 2019. Graph theory and the analysis of fracture networks. Journal of Structural Geology 125 155-165. https://doi.org/10.1016/j.jsg.2018.04.011.

Satoh, A., 2003. Introduction to Molecular-micro stimulation of Colloid Dispersions, in Satoh, A. Studies in Interference Science, Volume 17. Elsevier Science, eBook ISBN 9780444514240.

Silberschmidt, V.V., 1994. Fractal Characteristics of Joint Development in Stochastic Rocks pp 65 – 74. In Kruhl, J. H. (ed.), Fractals and Dynamic Systems in Geoscience. Springer-Verlag Berlin Heidelberg. http://dx.doi.org/10.1007/978-3-662-07304-9.

Tariq, W., Rehman, G., Ahmad, S., Khan, M.I., Khan, S.F., 2017. Fracture porosity of the Lockhart Formation in the Nizampur Basin, KP, Pakistan. SPE PAPG Annual Technical Conference, 2017, Islamabad, pp 361 – 374.

Walsh, J.J., Watterson, J., 1993. Fractal analysis of fracture patterns using the standard box-counting technique: valid and invalid methodologies. Journal of Structural Geology 15(12), 1509–1512.

Wandrey, C.J., Law, B.E., Shah, H.A., 2004. The Sembar Goru / Ghazij Composite Total Petroleum System, Indus and Sulaiman–Kirthar Geologic Ranges, Pakistan, and India. United States Geological Survey Bulletin 1: 1–20.

Watkins, H., Bond, C.E., Healy, D., Butler, R.W.H., 2015. Appraisal of fracture sampling methods and a new workflow to characterise heterogeneous fracture networks at outcrop. Journal of Structural Geology 72, 67-82.

Welch, M.J., Souque, C., Davis, R.K., Knipe, R.J., 2015. In Agar, S.M., Geiger, S. (eds) Fundamental Controls on Fluid Flow in Carbonates: Current Workflows to Emerging Technologies. https://doi.org/10.1144/SP406.5.

Wennberg, O. P., Svånå, T., Azizzadeh M., Aqrawi, A. M. M., Brockbank, P., Lyslo K. B., Ogilvie S., 2006. Fracture intensity vs. mechanical stratigraphy in platform top carbonates: the Aquitanian of the Asmari Formation, Khaviz Anticline, Zagros, SW Iran. Petroleum Geoscience 12(3), 235-246.

Williams, V.S., Pasha, M.K. Sheikh, I.M., 1997. Geologic Map of the Islamabad-Rawalpindi Area, Punjab, Northern Pakistan. U.S. Department of the Interior. U.S. Geological Survey. Open-File Report 99-47.

Wu, H., Pollard, D.D. 1995. An experimental study of the relationship between joint spacing and layer thickness. Journal of Structural Geology 17, 887– 905.

Yeats, R. S., Hussain, A., 1987. Timing of structural events in the Himalayan foothills of north-western Pakistan. Geological Society of America Bulletin 99, 161–176.

Zhang, Z., Xie, H., Zhang, R., Gao, M., Ai, T., Zha, E., 2020. Size and spatial fractal distributions of coal fracture networks under different mining-induced stress conditions. International Journal of Rock Mechanics and Mining Sciences 132, 104364. https://doi.org/10.1016/j.ijrmms.2020.104364.

Zhihui, N. Lichun, W. Ming-hui, W., Jing, Y., Qiang, Z., 2013. The Fractal Dimension of River Length Based on the Observed Data. Mathematical and Numerical Modelling of Flow and Transport 2013, Article ID 327297. https://doi.org/10.1155/2013/327297.

Appendix 1: Topological and fractal information of each measurement point at the various measurement sites.

Site	Structure	Circle	Orientation relative to bedding	Lst bed thick (m)	Shale bed thick (m)	% lst	e (edge)	x (cross cutting)	y (intersecting)	i (terminating)	Total	Connectivity	Fracture intensity	Fracture density	Mean trace length	No. tips	No. lines	No. branches	D
1	Fore-thrust	1	Perpendicular	1.55	0.05	85%	25	5	26	5	61	4.00	12.50	5.73	0.69	16	31	52	1.80
		2	Parallel	1.25	0.11	90%	34	24	21	30	109	3.53	17.00	11.94	0.45	26	51	95	1.84
		3	Perpendicular	1.22	0.09	80%	14	11	27	18	70	3.38	7.00	8.91	0.25	23	45	72	1.77
		4	Oblique	1.28	0.13	80%	21	10	30	14	76	3.64	10.50	8.59	0.39	22	44	72	1.76
		5	Perpendicular	1.47	0.22	80%	20	17	21	8	66	5.24	10.00	7.32	0.43	15	29	135	1.78
		6	Parallel	1.65	0.14	80%	28	19	16	8	71	5.83	14.00	6.84	0.65	12	24	66	1.72
		Ave		1.41	0.11	80%	24	14	24	14	76	4.27	11.83	8.22	0.48	19	37	82	1.78
		SD		0.16	0.04	4%	6	6	5	8	25	0.93	3.17	1.97	0.15	5	10	27	0.04
2	Fore-thrust	1	Parallel	0	0.25	15%	19	7	33	20	79	3.02	9.50	9.55	0.32	27	53	74	1.72
		2	Oblique	0.9	0.40	20%	42	22	46	5	115	5.33	21.00	11.62	0.58	34	68	116	1.96
		3	Perpendicular	0.55	0.33	35%	64	85	72	14	235	7.30	32.00	27.22	0.37	79	157	285	1.93
		4	Oblique	0.4	0.24	40%	67	65	78	19	229	5.90	33.50	25.78	0.41	72	143	257	1.92
		Ave		0.46	0.29	28%	48	45	57	15	165	5.39	24.00	18.54	0.42	53	105	183	1.88
		SD		0.07	0.12	10%	22	36	21	7	86	1.54	9.66	8.01	0.10	23	45	90	0.11
3	Fore-thrust	1	Perpendicular	1.45	0	100%	17	16	31	62	126	2.02	8.50	17.35	0.16	47	93	110	1.99
		2	Perpendicular	1.33	0	100%	16	4	28	4	52	4.00	8.00	5.73	0.44	16	32	52	1.95
		Ave		1.39	0	100%	17	10	30	33	90	3.01	8.25	11.54	0.30	31	63	81	1.97
		SD		0.06	0	0%	1	6	2	29	38	0.99	0.25	5.81	0.14	15	31	29	0.03
4	Pop-up	1	Perpendicular	0.31	0	100%	20	14	23	110	167	1.11	10.00	23.40	0.14	133	67	118	1.78
		2	Parallel	0.33	0	100%	14	5	15	110	144	0.64	7.00	20.69	0.11	125	63	88	1.77
		Ave		0.31	0	100%	17	10	19	110	156	0.88	8.50	22.04	0.12	129	65	103	1.78
		SD		0.01	0	0%	4	6	6	0	16	0.33	2.12	1.91	0.02	6	3	21	0.01
5	Back-thrust	1	Parallel	1.55	0.05	0%	55	64	114	181	414	2.41	27.50	57.14	0.15	295	148	390	1.93
		2	Oblique	1.40	0.05	0%	30	43	34	6	113	2.54	17.50	36.76	0.15	186	93	256	1.96
		3	Oblique	1.35	0.05	0%	42	48	46	14	150	2.89	17.00	19.74	0.27	101	51	147	1.91
		Ave		1.43	0.05	0%	42	52	65	67	226	2.61	20.67	37.88	0.19	194	97	264	1.93
		SD		0.05	0	0%	13	11	43	99	166	0.25	5.92	18.73	0.07	97	49	122	0.03
6	Back-thrust	1	Parallel	1.25	0	100%	24	18	29	132	203	1.17	12.00	28.49	0.13	161	81	225	1.87
		2	Oblique	0.95	0.02	80%	29	27	125	159	340	2.14	14.50	49.50	0.09	284	142	321	1.97
		3	Perpendicular	1.00	0.02	95%	27	6	51	88	172	1.64	13.50	23.08	0.19	139	70	133	1.95
		Ave		1.07	0.02	92%	27	17	68	126	238	1.65	13.33	33.69	0.14	195	97	226	1.93
		SD		0.16	0	10%	3	11	50	36	100	0.40	1.03	11.40	0.04	64	32	77	0.05
7	Back-thrust	1	Parallel	1.1	0	100%	24	66	55	76	221	3.69	12.00	31.35	0.12	61	121	253	1.83
8	Back- thrust	1	Parallel	0.9	0.01	95%	39	50	53	23	165	5.42	19.50	20.05	0.31	52	103	191	1.82
9	Pop-up	1	Parallel	0.5	0	100%	18	24	23	19	84	4.48	9.00	10.50	0.27	24	47	92	1.76
10	Fore- thrust	1	Parallel	0.4	0	100%	30	20	45	3	98	5.42	15.00	10.82	0.44	33	65	109	1.90